HIF1A-mediated pathways promote euploid cell survival in chromosomally mosaic embryos

Estefania Sanchez-Vasquez[1], Marianne E. Bronner[1] and Magdalena Zernicka-Goetz[1*]

[1]Division of Biology 139-74, California Institute of Technology, Pasadena, CA 91125, USA.

*Lead and correspondence: magdaz@caltech.edu

Running title
How embryos navigate chromosomal imbalance

Key words
Embryogenesis/ Aneuploidy/ Mosaic embryos/ DNA repair/ Hypoxia

ABSTRACT

Human fertility is suboptimal in part by error-prone divisions during early cleavage stages, which frequently result in chromosomal aneuploidy. Most human pre-implantation embryos are mosaics of euploid and aneuploid cells, yet those with a low proportion of aneuploid cells can develop to term at rates similar to fully euploid embryos. How embryos manage aneuploidy during early development remains poorly understood – yet this knowledge is crucial for improving fertility outcomes and reducing developmental defects. To investigate these mechanisms, we established a new mouse model of chromosome mosaicism to trace the fate of aneuploid cells during pre-implantation development. We previously used the Mps1 inhibitor reversine to induce aneuploidy. Here, we demonstrate that the more specific Mps1 inhibitor AZ3146 similarly disrupts chromosome segregation but supports higher developmental potential than reversine. AZ3146-treated embryos transiently upregulate Hypoxia Inducible-Factor-1A (HIF1A) without triggering p53 activation. Given that pre-implantation embryos develop in a hypoxic environment *in vivo*, we further explored the role of oxygen tension. Hypoxia exposure *in vitro* reduced DNA damage in response to Mps1 inhibition and increased the proportion of euploid cells in mosaic epiblast. Conversely, HIF1A inhibition decreased the proportion of aneuploid cells. Together, these findings uncover a role for hypoxia signaling in modulating the response to chromosomal errors and suggest new strategies to improve the developmental potential of mosaic human embryos.

INTRODUCTION

Humans have relatively low fertility compared to other mammals, with only ~30% of conceptions resulting in live birth (Palmerola et al., 2022a) Capalbo et al., 2021). A striking feature of early human development is the high frequency of chromosome segregation errors during cleavage stage divisions, leading to aneuploidy – the gain or loss of chromosomes (Allais & FitzHarris, 2022; Currie et al., 2022; Palmerola et al., 2022b; Pauerova et al., 2020; Vanneste et al., 2009). This high incidence of aneuploidy is thought to underlie low human fecundity and many developmental defects (Palmerola et al., 2022a). Both *in vivo* and *in vitro* fertilization (IVF) frequently results in embryos that are chromosomally mosaic, containing a mixture of diploid and aneuploid cells. It is estimated that ~60% of pre-implantation IVF embryos exhibit this form

of mosaicism (Capalbo et al., 2021). Despite its prevalence, our understanding of how embryos respond to and cope with aneuploidy during early development remains limited.

The incidence of aneuploidy declines at development progresses (Shahbazi et al., 2020; Yang et al., 2021), but the mechanism underlying this decline remains unclear. Remarkably, mosaic human embryos can develop to term (Capalbo et al., 2021; Greco et al., 2015; Starostik et al., 2020). Specifically, embryos classified as low- or medium-grade mosaics - defined by presence of 20-30% or 30-50% aneuploid cells in the trophectoderm – have implantation and birth rates comparable to fully euploid embryos (Capalbo et al., 2021). These observations raise a fundamental question: how do some mosaic embryos maintain developmental potential despite chromosomal abnormalities? Uncovering the mechanisms that support the viability of mosaic embryos is essential for improving reproductive outcomes and embryo selection strategies.

Mouse models of chromosome mosaicism provide a powerful system to investigate mechanisms that cannot be ethically studied in human embryos. Importantly, mouse and human pre-implantation development are highly similar: both undertake cleavage divisions, compaction, blastocyst cavity formation and hatching, albeit with slightly different timings (Mole et al., 2020; Zhu et al., 2021). During this period, outer cells differentiate into the extra-embryonic trophectoderm (TE), whereas inner cells form the inner cell mass (ICM), which further segregates into the embryonic epiblast (EPI) or extra-embryonic primitive endoderm (PE). The TE will form the placenta, the PE will form the yolk sac and the EPI will form the fetus (Zhu & Zernicka-Goetz, 2020).

Recently, our group developed the first mouse model of chromosome mosaicism by inducing aneuploidy using the small-molecule inhibitor reversine (Bolton et al., 2016; Singla et al., 2020). Reversine is a pan-Aurora kinase inhibitor that also antagonizes the A3 adenosine receptor and inhibits mitotic kinase monopolar spindle 1 (MPS1) (D'Alise et al., 2008; Santaguida et al., 2010). We found that reversine-treated mosaic embryos exhibit widespread aneuploidy and upregulation of p53 (Bolton et al., 2016). Importantly, aneuploid cells in mosaic embryos are progressively eliminated from the EPI, beginning around the time of implantation. Consistent with findings in human embryos (Capalbo et al., 2021), murine mosaic embryos containing at least 50% of euploid cells had a similar developmental potential to fully euploid embryos (Bolton et al., 2016; Singla et al., 2020).

However, because reversine affects p53 and may compromise cellular fitness (D'Alise et al., 2008; Santaguida et al., 2010), we sought to establish a complementary model using a more specific Mps1 inhibitor, AZ3146 (Hewitt et al., 2010). Although both AZ3146 and reversine interfere with the spindle assembly checkpoint, they bind to Mps1 in a different manner (Lan & Cleveland, 2010). In mouse embryos, AZ3146 treatment was shown to double the occurrence of micronuclei, indicative of chromosome segregation defects, but without impairing overall cellular fitness (Vazquez-Diez et al., 2019). In this study,

we use both AZ3146- and reversine-treated embryos to dissect the mechanisms governing aneuploid cell elimination and survival during pre-implantation development.

RESULTS

AZ3146 treatment induces chromosome segregation defects in pre-implantation embryos.

To generate distinct models of aneuploidy, we treated 4- to 8-cell stage mouse embryos with AZ3146 (20 μM) (Vazquez-Diez et al., 2019), as well as with reversine (0.5 μM) (Bolton et al., 2016) as a positive control, or DMSO (vehicle) as a negative control (Fig. 1A). We evaluated how the different Mps1 inhibitors affect chromosome segregation by detecting nuclei and kinetochores in 8-cell embryos and counted chromosomes *in situ* (Pauerova et al., 2020). Micronuclei were identified as small DAPI-stained chromosomes that were clearly distinct from the nuclei (Fig. S1A). We examined 32 DMSO-treated control embryos and observed only 22 cells with micronuclei out of a total of 256 cells (Fig. S1B). In contrast, we observed 82 cells with micronuclei in a total of 144 individual cells from 18 reversine-treated embryos, and 182 cells in a total of 304 individual cells from 38 AZ3146-treated embryos (Fig. S1A). After normalization, the average of aneuploidy in DMSO-treated 8-cell embryos was 12.5%, compared to 75% in the reversine-treated embryos and 62.5% in the AZ3146-treated embryos (Fig. S1B). We also detected non-dividing nuclei as rounded circles with distinct DAPI intensities in embryos treated with reversine and AZ3146. Specifically, we observed 28 non-dividing cells (19%) in reversine-treated embryos and 24 non-dividing cells (7.9%) in AZ3146-treated blastomeres, but none in DMSO-treated blastomeres (Fig. S1B). The increased frequencies of micronuclei and non-dividing cells in response to Mps1 inhibition are consistent with elevated aneuploidy and chromosomal instability (Daughtry and Chavez, 2016; Vazquez-Diez et al., 2016), as we showed previously for reversine-treated embryos (Bolton et al., 2016).

Given these distinct responses to reversine and AZ3146, we examined how these treatments impact the lineages in the blastocyst. To this end, we treated embryos with DMSO, reversine or AZ3146 from the 4- to 8-cell stage, and then washed and cultured them until the late blastocyst stage (E4.5). We assessed lineages by immunofluorescence (IF) to detect the TE marker CDX2, the EPI marker NANOG, and the PE marker SOX17. We found that all lineages segregated normally, and that blastocyst morphology was similar in all three conditions (Fig. 1B). We quantified the number of cells in the blastocysts and found that DMSO-treated controls had a median of 93 cells in total, whereas reversine- and AZ3146-treated embryos had a median of only 79 and 82 cells, respectively (n=28 embryos per treatment collected from three independent experiments. (Fig. 1C). DMSO-treated blastocysts contained a median of 15 EPI, 11 PE, and 67 TE cells, whereas reversine-treated blastocysts contained 12 EPI, 8 PE and 59 TE cells, and AZ3146-treated blastocysts had 11 EPI, 7 PE and 64 TE cells (Fig. 1C). These data suggest that reversine treatment compromises the development of all three lineages, as observed previously (Bolton et al., 2016), whereas AZ3146 mainly compromises ICM (EPI and PE) development (Statistical test: Mann–Whitney U-test).

116 To compare the developmental potential of blastocysts that had been treated with AZ3146 or reversine, we
117 transfer ~7 embryos per treatment into opposite uterine horns of the same mouse and counted decidua,
118 which reflect successful implantation, as well as viable embryos at E9.5. Although two (8%) reversine-
119 treated blastocysts developed decidua (Fig. S1C), none gave rise to viable E9.5 embryos. In contrast,
120 seven (30%) AZ3146-treated blastocysts developed decidua (Fig. S1C) and five (21%) generated viable
121 E9.5 embryos (Fig. S1D). Thus, AZ3146-treated embryos appear to have a higher developmental potential
122 than reversine-treated embryos.
123
124 Considering that cellular fitness and aneuploid stress are related to DNA damage and DNA repair, we first
125 sought to understand if these parameters were affected in our drug treatments. We used IF to quantify the
126 levels of the DNA repair marker PARP1 and of the DNA damage marker, phosphorylated H2A.X (γH2A.X)
127 at the 8-cell and morula stages (Fig. 1D). We observed elevated γH2A.X levels in reversine- and AZ3146-
128 treated 8-cell embryos compared to controls (Fig. 1E) (n=~15 embryos per treatment, ~120 cells. Collection
129 was made during three independent experiments. Statistical test: t-test), which eventually returned to
130 normal in AZ3146-treated blastocysts, but not in reversine-treated blastocysts (Fig. S2A).
131
132 PARP1 was specifically enriched in the EPI lineage in normal blastocysts, as assessed by IF (n>21 embryos
133 per treatment collected from three independent experiments Statistical test: Mann–Whitney U-test) and re-
134 analysis of published scRNA-seq data (Deng et al., 2014) (Fig. S2B). Intriguingly, PARP1 levels were
135 reduced at the 8-cell and morula stages in reversine-treated embryos compared to controls and to AZ3146-
136 treated embryos (Fig. 1 D-E). Moreover, late morula stage embryos treated with the PARP inhibitor Olaparib
137 (10 μM) (Hou et al., 2022; Prasad et al., 2017) developed into smaller blastocysts with only 78 total cells,
138 reflecting a relatively low number of ICM cells, only 8 EPI and 4 PE cells in DMSO-treated embryos (Fig.
139 S2C-E). Treatment with reversine, but not AZ3146, further reduced the number of cells in the EPI lineage
140 of Olaparib-treated embryos (Fig. S2E) (n=15 embryos per treatment collected from three independent
141 experiments. Statistical test: Mann–Whitney U-test). Overall, these data suggest that PARP1 is required for
142 proper development of the ICM, and that its reduced levels after reversine treatment may negatively impact
143 development.
144
145 **Reversine and AZ3146 activate distinct stress response pathways in pre-implantation embryos.**
146 Chromosome mis-segregation and aneuploidy are associated with different cellular stress pathways (Zhu
147 et al., 2018). For instance, p53 is frequently activated following DNA damage, which can limit proliferation
148 and trigger apoptosis (Abuetabh et al., 2022; Soto et al., 2017; Thompson & Compton, 2010). The p38
149 mitogen-activated protein kinase (MAPK) can also be activated following DNA damage (Thompson and
150 Compton, 2010). In aneuploid cells, p38 promotes apoptosis by inhibiting the transcription factor Hif-1α
151 (Simoes-Sousa et al., 2018), which otherwise promotes cell survival, proliferation, and metabolic changes

152 in aneuploid cells and in response to hypoxia in different contexts (Hu et al., 2003; Simoes-Sousa et al.,
153 2018).
154
155 To investigate how treatment with reversine or AZ3146 affect *p53* and *Hif1a* expression in mouse embryos,
156 we performed RT-qPCR at the morula and blastocyst stages. We normalized to *Ppia* (Peptidylprolyl
157 Isomerase A) mRNA, which is a stable reference gene in diploid and polyploid embryos (Gu et al., 2014).
158 Reversine-treated embryos displayed a significant increase in *p53* transcript levels at the morula (7-fold)
159 and blastocyst (1.3-fold) stages compared with DMSO-treated embryos (Sample: 3 biological replicates
160 and 2 technical replicates per experiment with each replicate having a minimum of 16 embryos. Statistical
161 test: Welch's t-test) (Fig. 2A), as we showed previously (Singla et al., 2020). In addition, reversine-treated
162 embryos showed reduced expression of *Hif1a* at the blastocyst stage, which would be consistent with p38
163 activation. In contrast, AZ3146-treated embryos did not show upregulation of *p53* at either the morula or
164 blastocyst stage (Fig. 2A). Moreover, AZ3146-treated embryos showed a transient increase in *Hif1a* mRNA
165 levels (3-fold) at the morula stage compared to DMSO- and reversine-treated embryos (Fig. 2A), which
166 returned to normal levels at the blastocyst stage. HIF1A protein was present in DMSO- and reversine-
167 treated embryos and elevated at the morula and blastocyst stages in AZ3146-treated embryos
168 (n=~20embryos per treatment. Statistical test: Mann–Whitney U-test, error bars represent s.e.m) (Fig. 2B).
169 HIF1A appeared to be mostly nuclear in morula, but mostly cytoplasmic in blastocysts, under all three
170 conditions (Fig. 2B). Overall, these data suggest that treatment with reversine, but not AZ3146, induces
171 multiple stress pathways in pre-implantation embryos. These differences may contribute to the increased
172 developmental potential of embryos treated with AZ3146 versus reversine.
173
174 **HIF1A activity is required for proper blastocyst formation after Mps1 inhibition.**
175 It was previously shown that Hif1α$^{-/-}$ embryos undergo developmental arrest and lethality by E11 (Iyer et
176 al., 1998). To assess the role of HIF1A in the embryo's response to reversine and AZ3146, we used a
177 pharmacological approach to inhibit its function. Briefly, we tested two different small molecules that have
178 been shown to inhibit HIF1A activity, PX-478 (Lee & Kim, 2011; Zhao et al., 2015) and IDF-11774 (Ban et
179 al., 2017). We treated control zygotes with DMSO, PX-478 (2 μM), or IDF-11774 (20 μM) until the blastocyst
180 stage (Fig. S3A). Unlike PX-478, IDF-11774 treatment did not significantly affect the total number of cells
181 in the TE or the whole blastocyst compared to the control (n=~12 embryos per treatment collected from
182 three independent experiments. Statistical test: Mann–Whitney U-test) (Fig. S3B). Therefore, we used IDF-
183 11774 to inhibit HIF1A in subsequent experiments.
184
185 Next, we treated embryos with DMSO, reversine, or AZ3146 from the 4- to 8-cell stage, washed them, and
186 then inhibited HIF1A with IDF-11774 from the 8-cell to blastocyst stage (Fig. 2C). Inhibition of HIF1A did
187 not abolish cavitation but dramatically lowered the number of TE and especially PE cells in AZ3146-treated
188 embryos compared to DMSO-treated controls (Fig. 2D) and compared to AZ3146-treated embryos not

exposed to IDF-11884 (Fig. 1C). Inhibition of HIF1A also lowered the number of cells in reversine-treated embryos compared to controls, but the effect was smaller (n=20 embryos per treatment collected from three independent experiments. Statistical test: Mann–Whitney U-test) (Fig. 2D). Overall, our data suggest that elevated HIF1A activity from the 8-cell stage onwards is particularly important to promote the survival of aneuploid TE and PE cells after AZ3146 treatment.

Taken together, our data suggest that AZ3146 and reversine have distinct effects on the pre-implantation embryo. Compared to reversine-treated embryos, AZ3146-treated embryos appear to have increased developmental potential, lack upregulation of p53, and show transient upregulation of *Hif1a*. Moreover, AZ3146-treated embryos have a greater dependence on HIF1A activity to form the TE and PE.

Hypoxia exposure attenuates DNA damage and blastomere defects in response to Mps1 inhibition. Pre-implantation development occurs in a hypoxic environment, and many clinics culture human embryos under hypoxic conditions (5%) (Houghton, 2021). It was reported that physiologic oxygen concentration (~5% oxygen) can improve the yield and quality of mammalian blastocysts (Ciray et al., 2009; Nguyen et al., 2020) and increase the nuclear translocation of HIF1A in mouse blastocysts (Choi et al., 2021) To investigate how hypoxia affects the development of euploid and aneuploid mouse embryos, we repeated our experiments performed under normoxia (20% O_2/5% CO_2; control) (Fig. 1A) in hypoxic (5% O_2/5% CO_2) conditions taking into consideration the standard practices in the IVF clinics (Knudtson et al., 2022) (Fig. 3A). We cultured embryos from the 2-cell stage until the blastocyst stage, treating them with DMSO, reversine, or AZ3146 from the 4-8 cell stage.

First, we examined lineage specification by quantifying the cell numbers in all three lineages at the blastocyst stage. We found that DMSO-treated blastocysts cultured under hypoxia had a median of 74 cells, representing 14 EPI cells, 6 PE cells and 54 TE cells (n=18 embryos per treatment collected from three independent experiments. Statistical test: Mann–Whitney U-test)(Fig. 3B-C). These data suggest that, under our conditions, the cell number in the pre-implantation mouse blastocyst is reduced when cultured in hypoxia compared to normoxia (Fig. 3C, 1C), particularly in the TE and PE. Notably, reversine and AZ3146 treatment did not further reduce cell numbers for embryos cultured under hypoxia, except for in the PE (Fig. 3C).

To investigate how hypoxia exposure affects DNA damage and repair in mouse embryos, we again performed IF for γH2A.X and PARP1 in 8-cell embryos and morula (Fig. 3D-E) (n=25 embryos per treatment collected from three independent experiments. Statistical test: t-test). We found that treated embryos with reversine and AZ3146 under hypoxia generated lower levels of γH2A.X (Fig. 3E) compared with the same treatments under normoxia (Fig. 1E). Whereas PARP1 levels at the 8-cell stage are reduce in reversine-treated embryos (Fig. 3E), similar to normoxic conditions (Fig. 1E). Importantly, at the morula stages, the

levels of PARP1 are relatively low compared to morula stage in normoxic conditions (Fig. 1E). Overall, these data suggest that hypoxia exposure lowers the accumulation of DNA damage between the 8-cell to morula stages, and results in a reduction of PARP1 at the morula stage.

Hypoxia increases the proportion of euploid cells in the epiblast of mosaic blastocysts.

Despite the high incidence of mosaicism in human pre-implantation embryos, the fate of aneuploid cells in mosaic embryos is incompletely understood. We previously used reversine to generate a mouse model of pre-implantation chromosome mosaicism and found that aneuploid (Reversine-treated) cells are eliminated in the EPI of mosaic embryos via apoptosis, starting from the mature blastocyst stage (Bolton et al., 2016). Whether this response reflects reversine treatment specifically, or aneuploidy more generally, is not known. Moreover, how hypoxia versus normoxia affects the outcomes is also not clear.

To address these questions, we created aggregation chimeras at the 8-cell stage that contained a 1:1 ratio of AZ3146-treated and control blastomeres (DMSO/AZ3146 chimeras), which is expected to reflect low-grade mosaicism, or of AZ3146-treated and reversine-treated blastomeres (reversine/AZ3146 chimeras), which is expected to reflect medium-grade mosaicism (Fig. 4A). We cultured these chimeric embryos in normoxia and hypoxia, and followed the fate of individual blastomeres by using transgenic mouse lines with the membrane markers mTmG (Muzumdar et al., 2007) and E-cadherin (Christodoulou et al., 2019). DMSO/AZ3146 and reversine/AZ3146 blastocysts displayed proper lineage allocation, embryo morphology and cavitation in both normoxia and hypoxia (Fig. 4B-C). In addition, DMSO/AZ3146 and reversine/AZ3146 embryos had comparable total cell numbers in their blastocysts, and blastocysts grown in hypoxia were again smaller than those grown in normoxia (Fig. 4D-E). Intriguingly, despite having fewer total cells, DMSO/AZ3146 blastocysts had more EPI cells when they were cultured in hypoxia compared to normoxia (Fig. 4D-E).

We quantified the proportion of AZ3146 cells in each lineage for each chimera. In DMSO/AZ3146-treated blastocysts, we found that 46.75% of the TE and 42.88% of the EPI originated from AZ3146-treated blastomeres, compared to only 28.57% of the PE (Fig. 4F). In reversine/AZ3146 chimeras, 63% of the TE and 78.4% of the EPI originated from AZ3146-treated cells, compared to only 40% of the PE (Fig. 4F). Thus, under normoxia, DMSO cells appear to outcompete AZ3146-treated cells, which in turn outcompete Reversine-treated cells in the TE and EPI. AZ3146-treated cells appeared to be at a competitive disadvantage in the PE in both contexts. Culturing DMSO/AZ3146 chimeras in hypoxia increased the representation of AZ3146-treated blastomeres in the TE (49.06%) and PE (50%) but, strikingly, reduced their representation in the EPI (33.3%) ($n>7$ embryos per treatment collected from three independent experiments. Statistical test: Mann–Whitney U-test) (Fig. 4G). These altered frequencies reflect a higher number of DMSO-treated cells in the EPI and a lower number in the PE (Fig. 4E). Hypoxia exposure of reversine/AZ3146 embryos lowered the contribution of AZ3146-treated blastomeres to the TE (55.94%)

263 and EPI (50%) but not the PE (46.43%) (Fig. 4G). We found that there was no correlation between the
264 proportion of AZ3146-treated cells in the TE and the EPI in DMSO/AZ3146 and reversine/AZ3146
265 aggregation chimeras, under hypoxia or normoxia, and that hypoxia seemed to have a greater impact on
266 the proportion of AZ3146 cells in reversine/AZ3146 aggregation chimeras (Fig. S4). Overall, these data
267 suggest that hypoxia has lineage-specific effects on competitions between aneuploid and euploid cells and
268 increases the contribution of euploid cells to the EPI.
269
270 Blastomeres in the 4-cell stage embryo display a lineage bias (Goolam et al., 2016). We considered that
271 mosaicism generated before the 4-cell stage might influence lineage allocation. To test this possibility, we
272 treated zygotes with reversine or AZ3146 during the first cleavage division. Importantly, reversine treatment
273 at the zygote stage seems to strongly affect the morphology of the blastocysts (Fig. S5A). Consistent with
274 this change in morphology, reversine-treatment reduced the number of cells in all lineages, particularly in
275 the TE and PE (Fig. S5B). In contrast, AZ3146 treatment did not affect morphology or cell number in any
276 of the lineages (Fig. S5A-B) (n=~27 embryos per treatment collected from three independent experiments.
277 Statistical test: Mann–Whitney U-test). To evaluate how early generation of aneuploidies in the embryos
278 affect cell competition, we generated DMSO/AZ3146, Reversine/DMSO, and Reversine/AZ3146
279 aggregation chimeras at the 2-cell stage and cultured them under normoxia until the blastocyst stage (Fig.
280 S5C). We found that all three 2-cell stage aggregation chimeras developed into blastocysts with proper
281 lineage segregation and the presence of a cavity (Fig. S5D). Interestingly, the reversine-treated cells were
282 extruded from the blastocyst in 54% of the reversine/DMSO chimeras and in 33% of the AZ3146/reversine
283 chimeras, whereas no cell extrusion was observed in the DMSO/AZ3146 chimeras. Quantification of the
284 proportion of AZ3146-treated cells in 2-cell stage derived chimeras (Fig. S5E) showed similar results as 8-
285 cell stage derived chimeras (Fig. 4F-G). In DMSO/AZ3146-treated blastocysts, we found that 49.28% of
286 the TE, 39% of the EPI and 33.33% of the PE originated from AZ3146-treated blastomeres (Fig. S5E). In
287 reversine/AZ3146 chimeras, 68.24% of the TE, 68.83% of the EPI, and 66.67% of the PE originated from
288 AZ3146-treated cells (Fig. S5E). In DMSO/reversine chimeras, 22.27% of the TE, 26.98% of the PE, and
289 31.7% of the EPI originated from reversine-treated cells. Overall, these results suggest that aneuploidy
290 generated at different stages similarly affect the proportion of aneuploid cells in the blastocysts.
291
292 **HIF1A inhibition reduces the frequency of aneuploid cells in DMSO/AZ3146 mosaic embryos.**
293 Our data suggest that hypoxia affects aneuploid-euploid cell competition in mosaic embryos (Fig. 4). To
294 further assess the effect of HIF1A and, considering most human embryos are culture under hypoxic
295 conditions, we decided to evaluate the effect of inhibiting HIF1A in mosaic embryos cultured in hypoxic
296 conditions. We assembled DMSO/AZ3146 and Reversine/AZ3146 8-cell stage chimeras, treated them with
297 the HIF1A inhibitor IDF-11774 (Fig. 5A, S6A-B), and then assessed lineage allocation in blastocysts.
298 Treatment of DMSO/AZ3146 chimeras with IDF11774 does not affect lineage segregation in the blastocyst
299 but reduces the cavity diameter (Fig. 5B-C). Additionally, diminish the contribution of AZ3146-treated cells

300 to the TE, but DMSO-treated cells seem to compensate for this loss in the PE and EPI (Fig. 5D, Fig. S6C).
301 Treating Reversine/AZ3146 chimeras with IDF11774 compromised blastocyst morphology and cavitation
302 (Fig. 5E-F) and considerable increased the number of PE and EPI cells (n>8 embryos per treatment
303 collected from three independent experiments. Statistical test: Mann–Whitney U-test) (Fig. 5G), without
304 altering the frequency of AZ3146-treated cells (Fig. S6D). Taken together, our data suggest that HIF1A
305 promotes the survival of AZ3146-treated cells in DMSO/AZ3146 chimeras and suggest that inhibiting HIF1A
306 could increase the proportion of karyotypically normal cells in mosaic embryos.
307
308 **DISCUSSION**
309 Aneuploidy is a frequent outcome of early embryonic divisions (Allais & FitzHarris, 2022; Currie et al., 2022;
310 Palmerola et al., 2022b). Here, we describe complementary strategies for inducing aneuploidy in mouse
311 embryos and reveal how the embryo's response varies depending on the nature of the insult, clel lineage,
312 and environmental context. Our findings support four key conclusions: 1) the Mps1 inhibitor AZ3146 induces
313 aneuploidy while preserving DNA repair capacity and dampening stress responses, compared to the
314 broader-acting inhibitor reversine; 2) Lineage specific responses to aneuploidy emerge during blastocyst
315 development, consistent with our earlier findings (Bolton et al., 2016; Singla et al., 2020); 3) HIF1A
316 promotes survival of extraembryonic lineages (TE and PE) in AZ3146-treated embryos, whereas PARP1 is
317 particularly required in the EPI of both AZ3146- and reversine-treated embryos; 4) Hypoxia enhances DNA
318 repair and influences the competitive dynamics between aneuploid and euploid cells in mosaic embryos.
319
320 Reversine-treated embryos upregulate mRNA levels of senescent markers p53 and p21 (Singla et al., 2020)
321 and fail to give rise to viable embryos (Bolton et al., 2016). Our current results further indicate that reversine
322 downregulates PARP1, consistent with previous findings in glioma cells (Hirakata et al., 2021), thereby
323 exacerbating DNA damage and limiting DNA repair capacity. In contrast, AZ3146-treated embryos maintain
324 PARP1 expression and exhibit increased HIF1A activity, which appears to support the survival of extra-
325 embryonic lineages and improve overall developmental potential.

326 These findings intersect with a broader conversation about embryo culture conditions. It has been proposed
327 that standard culture practices shift from normoxia (20% oxygen) to more physiological hypoxia (5%
328 oxygen) to better recapitulate the *in vivo*-like oviductal environment (Alva et al., 2022). Indeed, hypoxic
329 culture conditions have been shown to improve the quality of mammalian blastocysts (Ciray et al., 2009;
330 Nguyen et al., 2020), though the underlying mechanisms remain unclear. Studies in somatic cells suggest
331 that hypoxia enhances DNA repair pathways (Marti et al., 2021; Nakamura et al., 2022; Pietrzak et al.,
332 2018). In line with this, we observed reduced DNA damage in aneuploid embryos cultured under hypoxic
333 conditions, consistent with prior reports of lower γH2A.X levels in mouse blastocysts recovered from the
334 uterus or cultured in low oxygen (Houghton, 2021; Meuter et al., 2014). Furthermore, recent work in cancer
335 cells indicates that hypoxia may promote HIF1A-PARP1 interactions, enhancing DNA repair (Marti et al.,
336 2021; Nakamura et al., 2022; Pietrzak et al., 2018). Together, these findings highlight the interplay between

337 chromosomal stress, lineage context, and the embryonic microenvironment in shaping cell fate during early
338 development. A deeper mechanistic understanding of how DNA repair is regulated at pre-implantation
339 stages will be crucial for elucidating how embryos tolerate or eliminate aneuploid cells — with important
340 implications for improving embryo culture systems and fertility treatments.

341 Confined placental mosaicism, in which the placenta is aneuploid while the foetus is euploid, is a common
342 phenomenon in human pregnancies (McCoy, 2017). In previous work, we showed that aneuploid TE cells
343 exhibit prolonged cell cycles and signs of senescence, whereas aneuploid ICM cells have an increased
344 frequency of apoptosis in reversine-treated embryos (Singla et al., 2020). These findings suggest that
345 abnormal, yet viable TE cells, may contribute to confined placental mosaicism. In the present study, we
346 found that in AZ3146-treated embryos cultured under normoxic conditions, aneuploid cells contributed
347 predominantly to the TE, followed by the EPI, and were especially depleted from the PE. Under hypoxic
348 conditions, however, we observed a shift: aneuploid cells were more frequently eliminated from the EPI and
349 enriched in the PE. These observations suggest that hypoxia modulates lineage-specific cell competition
350 in mosaic embryos, potentially promoting a higher proportion of euploid cells in the EPI relative to the PE
351 and TE. Moreover, we confirmed that the proportions of aneuploid cells in the TE and EPI do not correlate,
352 consistent with the preferential survival of aneuploid cells in the TE and their selective elimination from the
353 ICM. This is in line with clinical data showing low concordance of aneuploidy between TE and ICM in human
354 mosaic embryos (30–40%) (Dahdouh & Garcia-Velasco, 2021). Lineage-specific elimination of aneuploid
355 cells by apoptosis has been described in an *in vitro* model of human post-implantation development using
356 reversine (Yang et al., 2021). Our findings mirror this distinction and further suggest that mechanisms of
357 DNA repair—possibly involving PARP1 and HIF1A—may underlie the differential survival of aneuploid cells
358 across lineages. Investigating how these pathways operate during post-implantation development will be
359 crucial for understanding the developmental trajectories of mosaic embryos and the basis of placental
360 mosaicism.

361 Since low- and medium- grade mosaic human embryos have similar developmental potential to fully euploid
362 embryos (Capalbo et al., 2021; Greco et al., 2015), understanding the molecular pathways that govern the
363 response to aneuploidy holds important translational promise. Given that the extent and proportion of
364 aneuploid cells in mosaic embryos impact embryo viability (Capalbo et al., 2021), strategies that reduce the
365 aneuploid cell burden at the blastocyst stage may enhance the likelihood of a successful pregnancy. In this
366 study, we targeted HIF1A as a potential regulator of aneuploid cell persistence and found that treatment
367 with the HIF1A inhibitor IDF-11774 increased the proportion of euploid cells in mosaic embryos. Taken
368 together, our findings reveal that specific environmental and molecular factors can modulate the
369 composition of mosaic embryos, with potential implications for improving embryo quality and reproductive
370 outcomes.

371

372 **MATERIALS AND METHODS**

373 **Pre-implantation embryo culture**

374 Mice were maintained according to national and international guidelines. Four- to six-week-old B6SJLF1/J
375 female mice were injected with 7.5 IU PMSG followed by 7.5 IU hCG 48 h later, to induce superovulation.
376 The females were then mated with B6CBAF1/J males or were indicated, with E-cadherin GFP or mTmG
377 transgenic males. Pre-implantation mouse embryos were recovered 24 h and 40 h after the hCG injection
378 to obtain zygotes and 2-cell stage embryos, respectively in M2 medium (Sigma, M7167). We incubate the
379 embryos in KSOM until 4-cell stage for the aneuploid treatment, around 53 h post hCG. When recovering
380 zygotes, cumulus cells were removed with 0.3% hyaluronidase (Sigma, H4272) in M2. Embryos were
381 cultured in regular KSOM (Sigma. MR-106) at 37°C under 5% CO_2/air (Normoxia) or with pre-mixed 5%
382 CO_2/ 5% O_2 balance with nitrogen, biologic atmosphere batch (Airgas #Z03NI9022000033) (Hypoxia).
383 Normoxia in our study was defined as the standard atmospheric oxygen levels in culture incubators (Alva
384 et al., 2022), whereas hypoxia (5% oxygen concentration) was the standard level of oxygen in the IVF
385 clinics and can be used to better model physiological oxygen (physoxia), which varies from ~1.5% to 8%
386 (Alva et al., 2022; Knudtson et al., 2022). B6SJLF1/J females and B6CBAF1/J males were obtained from
387 JAX laboratories. Females were received at 3-4 weeks of age and were maintained in the CALTECH animal
388 facility, where they were housed with 5 same-sex littermates on a 12 h light/12 h dark cycle with food and
389 water *ad libitum*. The temperature in the facility was controlled and maintained at 21 °C. All experimental
390 procedures involving the use of live animals, or their tissues were performed in accordance with the NIH
391 guidelines and approved by the Institutional Animal Care and Use Committee (IACUC) and the Institutional
392 Biosafety Committee at the California Institute of Technology (Caltech, protocol number 1772). Reversine
393 (Sigma, R3904), AZ3146 (Sigma, SML1427), PX-478 (Selleckchem, S7612), IDF-11774 (Selleckchem,
394 S8771) and olaparib (Selleckchem, S1060) were dissolved in DMSO (Sigma, D2650) before use to specific
395 concentration. They were respectively used at following final concentrations: 0.5 μM, 20 μM, 2 μM, 20 μM
396 and 10 μM. Control embryos were incubated in the equivalent DMSO concentration. Drugs were dissolved
397 in regular KSOM to the concentration of use. DMSO concentration in media should never pass 0.4%.
398

399 **Immunofluorescence**

400 Embryos were fixed in 4% PFA (Thermo Scientific, AA47340) for 20 min at room temperature (RT).
401 Following by three washes with 0.1% Tween-20 (Sigma, P1379) dissolved in PBS (PBST). The embryos
402 were then permeabilized with 0.3%, Triton X-100 (Sigma, X100) in PBS. Washes were then performed
403 three times in PBST before embryos were transferred to blocking solution (3% BSA in PBS) for at least 3h
404 at RT. Incubation with primary antibodies was performed in blocking solution overnight at 4°C. Next day,
405 washes were performed three times in PBST before incubation with Alexa Fluor secondary antibodies
406 (Thermo Fisher Scientific, 1:500) in blocking solution for 2 h. Washes were performed three times before
407 incubation with DAPI (Thermo Fisher Scientific) for 5 min. Washes after DAPI were perform two times in
408 PBST before the final incubation in M2. Embryos were then mounted in M2 micro-drops on 35 mm glass

409 bottom dish (MATTEK, P35G-1.5-14-C). Confocal imaging was carried out using Leica SP8, 40x objective,
410 1 µM Z-step. Image files were viewed and analyzed using ImageJ and IMARIS 9.9 software.
411 Primary antibodies used: mouse anti-CDX2 (Biogenex, 1:500), rabbit anti-NANOG (1:500; Abcam), goat
412 anti-SOX17 (1:300; R&D Systems), rabbit anti-HIF1A (1:300, Novusbio), mouse anti-PARP1 (1:500,
413 Proteintech) and rabbit anti- Phospho- Histone H2AX (1:500, R&D Systems).
414
415 ***In situ* chromosome counting**
416 For determination of aneuploidy, treated 8-cell stage embryos were synchronized in metaphase by 10h
417 treatment with 0.03 µg/mL colcemid (Cayman, 15364) diluted in KSOM. Following by 1h treatment with 10
418 µM Mg132 (Selleckchem, S2619) in KSOM. Finally, 1 h treatment with 5 µM dimethylenastron
419 (MedChemExpress, HY-19944) and 10 µM Mg132 in KSOM. Synchronized embryos were then fix in 2%
420 PFA for 20 min, permeabilized with PBST for 15 min and blocked 3h at RT before incubation with human
421 anti-centromere protein antibody (1:300, Antibodiesinc 15-234) overnight at 4°C. Next day, three washes
422 with PBST were performed before 2 h incubation with goat anti-Human secondary antibody, Alexa Fluor
423 647 (1:400, Invitrogen A-21445) in blocking solution. Washes were performed three times before 20 min
424 incubation with DAPI (1:500) and Alexa Fluor 488 Phalloidin (1:300, Invitrogen A12379). Washes then were
425 performed three times before clearing overnight with AF1 plus (Citifluor, AF1/DAPI-15). Embryos were then
426 mounted in AF1 plus micro-drops on 35 mm glass bottom. Confocal imaging was carried out using Leica
427 SP8, 60x objective, 0.5 µM Z-step. Image files were viewed and analyzed using ImageJ and IMARIS 9.9
428 software.
429
430 **Embryo transfers and post implantation recovery and biopsy**
431 Embryo transfer were performed as described previously (Bermejo-Alvarez et al., 2014). CD1 females and
432 vasectomizes CD1 males were obtained from Charles River. Reversine and AZ3146-treated blastocyst
433 were transfer into 2.5-days pseudopregnant CD1 females. Around 16 AZ3146-treated embryos were
434 transfer in the right uterine horn, whereas around 16 reversine-treated embryos were transfer in the left
435 uterine horn of the same female as control. To evaluate implantation and embryo survival potency, uterine
436 horns were recovered 5 days after surgery. Deciduas were dissected and post implantation embryos at
437 stage E9.5 were recovered into PBST on ice. Embryos were fixed in 4% PFA at RT for 1 h, followed by
438 washes through PBST before imaging. Images were taken using an Olympus LS stereo microscope with a
439 10x objective. Uterine transfers were performed in accordance with the NIH guidelines and approved by
440 the Institutional Animal Care and Use Committee (IACUC) and the Institutional Biosafety Committee at the
441 California Institute of Technology (CALTECH).
442
443 **qRT-PCR**
444 Around 14 to 17 morulas and blastocysts were collected for quantitative reverse transcriptase polymerase
445 chain reaction (qRT-PCR). Total RNA from morulas was obtained using the NucleoSpin RNA Plus XS kit

446 (Takara, 740990.10). Whereas total RNA from blastocyst was extracted using the Arcturus PicoPure RNA
447 Isolation Kit (Thermo Fisher, KIT0204). qRT-PCR was performed using the *Power* SYBR Green RNA-to-
448 CT 1-Step Kit (Applied Biosystems, 4389986) in a StepOne Plus Real-time PCR machine (Applied
449 Biosystems). The following program was used: 30 min 48 °C (reverse-transcription) followed by 10 min 95
450 °C followed by 45 cycles of 15 s 95 °C (denaturing) and 1 min 60 °C (annealing and extension). The ddCT
451 method was used to determine relative levels of mRNA expression, with Ppia as an endogenous control
452 (Gu et al., 2014). Primers were obtained from IDT.

Name	**Sequence**
p53_Fw	GTCACAGCACATGACGGAGG
p53_Rv	TCTTCCAGATGCTCGGGATAC
Hif1a_Fw	CCTGCACTGAATCAAGAGGTTGC
Hif1a_Rv	CCATCAGAAGGACTTGCTGGCT
Ppia_Fw	GAGCTCTGAGCACTGGAGAGA
Ppia_Rv	CCACCCTGGCACATGAAT

453

454 **Generation of chimeric embryos**

455 Chimeric embryos were generated following a previous publish protocol (Eakin & Hadjantonakis, 2006).
456 Briefly, wild-type, E-cadherin GFP or mTmG 8-cell stage embryos were transfer to micro-drops of M2 after
457 aneuploid treatment. Zona pellucida was removed by treatment with acidic Tyrode's solution (Sigma,
458 T1788). The embryos were then incubated in Ca2+/Mg2+-free M2 (made in house) for 5 min and then
459 disaggregated into individual blastomeres by gentle mouth pipetting. Mosaic chimeras were form by
460 aggregation of four and four (1:1) of each treatment. Low mosaicism DMSO/AZ3146-treated blastomeres
461 (1:1). Whereas medium mosaicism Reversine/AZ3146-treated blastomeres (1:1). Culture of the chimeras
462 were performed under normoxic and hypoxia condition in KSOM for 48 h to reach blastocyst stage.

463 **Statistical analysis**

464 The statistical tests used are indicated in the corresponding figure legends. Calculations were carried out
465 in Microsoft Excel and data analysis and visualization in Prism 9 software. All graphs show mean values,
466 error bars: s.e.m.

467

468 **AUTHOR CONTRIBUTIONS**

469 E.S.V designed and conducted the experiments; analyzed and interpreted the data. E.S.V and M.Z.G
470 conceived the project. M.E.B and M.Z.G supervised the study.

471

472 **ACKNOWLEDGEMENTS**

473 This work was supported by M.Z.G' National Institutes of Health R01 (R01HD101489) grant. E.S.V. is
474 supported by a Pew Latin America fellowship. We thank the Life Science Editors and the Life Science
475 Editors Foundation for invaluable comments and suggestions on the manuscript, and Ariane Helou for copy

editing. Data analysis was performed in the Biological Imaging Facility, with the support of the Caltech Beckman Institute and the Arnold and Mabel Beckman Foundation.

DECLARATION OF INTERESTS

The authors declare that they have no conflicts of interest.

REFERENCES

Abuetabh, Y., Wu, H. H., Chai, C., Al Yousef, H., Persad, S., Sergi, C. M., & Leng, R. (2022). DNA damage response revisited: the p53 family and its regulators provide endless cancer therapy opportunities. *Exp Mol Med*, *54*(10), 1658-1669. https://doi.org/10.1038/s12276-022-00863-4

Allais, A., & FitzHarris, G. (2022). Absence of a robust mitotic timer mechanism in early preimplantation mouse embryos leads to chromosome instability. *Development*, *149*(13). https://doi.org/10.1242/dev.200391

Alva, R., Gardner, G. L., Liang, P., & Stuart, J. A. (2022). Supraphysiological Oxygen Levels in Mammalian Cell Culture: Current State and Future Perspectives. *Cells*, *11*(19). https://doi.org/10.3390/cells11193123

Ban, H. S., Kim, B. K., Lee, H., Kim, H. M., Harmalkar, D., Nam, M., Park, S. K., Lee, K., Park, J. T., Kim, I., Lee, K., Hwang, G. S., & Won, M. (2017). The novel hypoxia-inducible factor-1alpha inhibitor IDF-11774 regulates cancer metabolism, thereby suppressing tumor growth. *Cell Death Dis*, *8*(6), e2843. https://doi.org/10.1038/cddis.2017.235

Bermejo-Alvarez, P., Park, K. E., & Telugu, B. P. (2014). Utero-tubal embryo transfer and vasectomy in the mouse model. *J Vis Exp*(84), e51214. https://doi.org/10.3791/51214

Bolton, H., Graham, S. J. L., Van der Aa, N., Kumar, P., Theunis, K., Fernandez Gallardo, E., Voet, T., & Zernicka-Goetz, M. (2016). Mouse model of chromosome mosaicism reveals lineage-specific depletion of aneuploid cells and normal developmental potential. *Nat Commun*, *7*, 11165. https://doi.org/10.1038/ncomms11165

Capalbo, A., Poli, M., Rienzi, L., Girardi, L., Patassini, C., Fabiani, M., Cimadomo, D., Benini, F., Farcomeni, A., Cuzzi, J., Rubio, C., Albani, E., Sacchi, L., Vaiarelli, A., Figliuzzi, M., Findikli, N., Coban, O., Boynukalin, F. K., Vogel, I., . . . Simon, C. (2021). Mosaic human preimplantation embryos and their developmental potential in a prospective, non-selection clinical trial. *Am J Hum Genet*, *108*(12), 2238-2247. https://doi.org/10.1016/j.ajhg.2021.11.002

Choi, J., Kim, W., Yoon, H., Lee, J., & Jun, J. H. (2021). Dynamic Oxygen Conditions Promote the Translocation of HIF-1alpha to the Nucleus in Mouse Blastocysts. *Biomed Res Int*, *2021*, 5050527. https://doi.org/10.1155/2021/5050527

Christodoulou, N., Weberling, A., Strathdee, D., Anderson, K. I., Timpson, P., & Zernicka-Goetz, M. (2019). Morphogenesis of extra-embryonic tissues directs the remodelling of the mouse embryo at implantation. *Nat Commun*, *10*(1), 3557. https://doi.org/10.1038/s41467-019-11482-5

Ciray, H. N., Aksoy, T., Yaramanci, K., Karayaka, I., & Bahceci, M. (2009). In vitro culture under physiologic oxygen concentration improves blastocyst yield and quality: a prospective randomized survey on sibling oocytes. *Fertil Steril*, *91*(4 Suppl), 1459-1461. https://doi.org/10.1016/j.fertnstert.2008.07.1707

Currie, C. E., Ford, E., Benham Whyte, L., Taylor, D. M., Mihalas, B. P., Erent, M., Marston, A. L., Hartshorne, G. M., & McAinsh, A. D. (2022). The first mitotic division of human embryos is highly error prone. *Nat Commun*, *13*(1), 6755. https://doi.org/10.1038/s41467-022-34294-6

D'Alise, A. M., Amabile, G., Iovino, M., Di Giorgio, F. P., Bartiromo, M., Sessa, F., Villa, F., Musacchio, A., & Cortese, R. (2008). Reversine, a novel Aurora kinases inhibitor, inhibits colony formation of human acute myeloid leukemia cells. *Mol Cancer Ther*, *7*(5), 1140-1149. https://doi.org/10.1158/1535-7163.MCT-07-2051

Dahdouh, E. M., & Garcia-Velasco, J. A. (2021). Embryos with mosaic results: busting the myth! *Reprod Biomed Online*, *43*(1), 1-2. https://doi.org/10.1016/j.rbmo.2021.04.015

526 Eakin, G. S., & Hadjantonakis, A. K. (2006). Production of chimeras by aggregation of embryonic stem
527 cells with diploid or tetraploid mouse embryos. *Nat Protoc*, *1*(3), 1145-1153.
528 https://doi.org/10.1038/nprot.2006.173
529 Goolam, M., Scialdone, A., Graham, S. J. L., Macaulay, I. C., Jedrusik, A., Hupalowska, A., Voet, T.,
530 Marioni, J. C., & Zernicka-Goetz, M. (2016). Heterogeneity in Oct4 and Sox2 Targets Biases Cell
531 Fate in 4-Cell Mouse Embryos. *Cell*, *165*(1), 61-74. https://doi.org/10.1016/j.cell.2016.01.047
532 Greco, E., Minasi, M. G., & Fiorentino, F. (2015). Healthy Babies after Intrauterine Transfer of Mosaic
533 Aneuploid Blastocysts. *N Engl J Med*, *373*(21), 2089-2090.
534 https://doi.org/10.1056/NEJMc1500421
535 Gu, Y., Shen, X., Zhou, D., Wang, Z., Zhang, N., Shan, Z., Jin, L., & Lei, L. (2014). Selection and
536 expression profiles of reference genes in mouse preimplantation embryos of different ploidies at
537 various developmental stages. *PLoS One*, *9*(6), e98956.
538 https://doi.org/10.1371/journal.pone.0098956
539 Hewitt, L., Tighe, A., Santaguida, S., White, A. M., Jones, C. D., Musacchio, A., Green, S., & Taylor, S. S.
540 (2010). Sustained Mps1 activity is required in mitosis to recruit O-Mad2 to the Mad1-C-Mad2 core
541 complex. *J Cell Biol*, *190*(1), 25-34. https://doi.org/10.1083/jcb.201002133
542 Hirakata, C., Lima, K., De Almeida, B. O., De Miranda, L. B. L., Florencio, K. G. D., Furtado, L. C., Costa-
543 Lotufo, L. V., & Machado-Neto, J. A. (2021). Targeting glioma cells by antineoplastic activity of
544 reversine. *Oncol Lett*, *22*(2), 610. https://doi.org/10.3892/ol.2021.12871
545 Houghton, F. D. (2021). HYPOXIA AND REPRODUCTIVE HEALTH: Hypoxic regulation of
546 preimplantation embryos: lessons from human embryonic stem cells. *Reproduction*, *161*(1), F41-
547 F51. https://doi.org/10.1530/REP-20-0322
548 Hu, C. J., Wang, L. Y., Chodosh, L. A., Keith, B., & Simon, M. C. (2003). Differential roles of hypoxia-
549 inducible factor 1alpha (HIF-1alpha) and HIF-2alpha in hypoxic gene regulation. *Mol Cell Biol*,
550 *23*(24), 9361-9374. https://doi.org/10.1128/MCB.23.24.9361-9374.2003
551 Iyer, N. V., Kotch, L. E., Agani, F., Leung, S. W., Laughner, E., Wenger, R. H., Gassmann, M., Gearhart,
552 J. D., Lawler, A. M., Yu, A. Y., & Semenza, G. L. (1998). Cellular and developmental control of
553 O2 homeostasis by hypoxia-inducible factor 1 alpha. *Genes Dev*, *12*(2), 149-162.
554 https://doi.org/10.1101/gad.12.2.149
555 Knudtson, J. F., Robinson, R. D., Sparks, A. E., Hill, M. J., Chang, T. A., & Van Voorhis, B. J. (2022).
556 Common practices among consistently high-performing in vitro fertilization programs in the United
557 States: 10-year update. *Fertil Steril*, *117*(1), 42-50. https://doi.org/10.1016/j.fertnstert.2021.09.010
558 Lan, W., & Cleveland, D. W. (2010). A chemical tool box defines mitotic and interphase roles for Mps1
559 kinase. *J Cell Biol*, *190*(1), 21-24. https://doi.org/10.1083/jcb.201006080
560 Lee, K., & Kim, H. M. (2011). A novel approach to cancer therapy using PX-478 as a HIF-1alpha inhibitor.
561 *Arch Pharm Res*, *34*(10), 1583-1585. https://doi.org/10.1007/s12272-011-1021-3
562 Marti, J. M., Garcia-Diaz, A., Delgado-Bellido, D., O'Valle, F., Gonzalez-Flores, A., Carlevaris, O.,
563 Rodriguez-Vargas, J. M., Ame, J. C., Dantzer, F., King, G. L., Dziedzic, K., Berra, E., de Alava,
564 E., Amaral, A. T., Hammond, E. M., & Oliver, F. J. (2021). Selective modulation by PARP-1 of
565 HIF-1alpha-recruitment to chromatin during hypoxia is required for tumor adaptation to hypoxic
566 conditions. *Redox Biol*, *41*, 101885. https://doi.org/10.1016/j.redox.2021.101885
567 McCoy, R. C. (2017). Mosaicism in Preimplantation Human Embryos: When Chromosomal Abnormalities
568 Are the Norm. *Trends Genet*, *33*(7), 448-463. https://doi.org/10.1016/j.tig.2017.04.001
569 Meuter, A., Rogmann, L. M., Winterhoff, B. J., Tchkonia, T., Kirkland, J. L., & Morbeck, D. E. (2014).
570 Markers of cellular senescence are elevated in murine blastocysts cultured in vitro: molecular
571 consequences of culture in atmospheric oxygen. *J Assist Reprod Genet*, *31*(10), 1259-1267.
572 https://doi.org/10.1007/s10815-014-0299-8
573 Mole, M. A., Weberling, A., & Zernicka-Goetz, M. (2020). Comparative analysis of human and mouse
574 development: From zygote to pre-gastrulation. *Curr Top Dev Biol*, *136*, 113-138.
575 https://doi.org/10.1016/bs.ctdb.2019.10.002
576 Muzumdar, M. D., Tasic, B., Miyamichi, K., Li, L., & Luo, L. (2007). A global double-fluorescent Cre
577 reporter mouse. *Genesis*, *45*(9), 593-605. https://doi.org/10.1002/dvg.20335
578 Nakamura, H., Sekine, H., Kato, H., Masai, H., Gradin, K., & Poellinger, L. (2022). Hypoxia-inducible
579 factor-1alpha and poly [ADP ribose] polymerase 1 cooperatively regulate Notch3 expression
580 under hypoxia via a noncanonical mechanism. *J Biol Chem*, *298*(7), 102137.
581 https://doi.org/10.1016/j.jbc.2022.102137

582 Nguyen, A. Q., Bardua, I., Greene, B., Wrenzycki, C., Wagner, U., & Ziller, V. (2020). Mouse embryos
583 exposed to oxygen concentrations that mimic changes in the oviduct and uterus show
584 improvement in blastocyst rate, blastocyst size, and accelerated cell division. *Reprod Biol*, *20*(2),
585 147-153. https://doi.org/10.1016/j.repbio.2020.03.011
586 Palmerola, K. L., Amrane, S., De Los Angeles, A., Xu, S., Wang, N., de Pinho, J., Zuccaro, M. V.,
587 Taglialatela, A., Massey, D. J., Turocy, J., Robles, A., Subbiah, A., Prosser, B., Lobo, R., Ciccia,
588 A., Koren, A., Baslan, T., & Egli, D. (2022a). Replication stress impairs chromosome segregation
589 and preimplantation development in human embryos. *Cell*.
590 https://doi.org/10.1016/j.cell.2022.06.028
591 Palmerola, K. L., Amrane, S., De Los Angeles, A., Xu, S., Wang, N., de Pinho, J., Zuccaro, M. V.,
592 Taglialatela, A., Massey, D. J., Turocy, J., Robles, A., Subbiah, A., Prosser, B., Lobo, R., Ciccia,
593 A., Koren, A., Baslan, T., & Egli, D. (2022b). Replication stress impairs chromosome segregation
594 and preimplantation development in human embryos. *Cell*, *185*(16), 2988-3007 e2920.
595 https://doi.org/10.1016/j.cell.2022.06.028
596 Pauerova, T., Radonova, L., Kovacovicova, K., Novakova, L., Skultety, M., & Anger, M. (2020).
597 Aneuploidy during the onset of mouse embryo development. *Reproduction*, *160*(5), 773-782.
598 https://doi.org/10.1530/REP-20-0086
599 Pietrzak, J., Spickett, C. M., Ploszaj, T., Virag, L., & Robaszkiewicz, A. (2018). PARP1 promoter links cell
600 cycle progression with adaptation to oxidative environment. *Redox Biol*, *18*, 1-5.
601 https://doi.org/10.1016/j.redox.2018.05.017
602 Santaguida, S., Tighe, A., D'Alise, A. M., Taylor, S. S., & Musacchio, A. (2010). Dissecting the role of
603 MPS1 in chromosome biorientation and the spindle checkpoint through the small molecule
604 inhibitor reversine. *J Cell Biol*, *190*(1), 73-87. https://doi.org/10.1083/jcb.201001036
605 Shahbazi, M. N., Wang, T., Tao, X., Weatherbee, B. A. T., Sun, L., Zhan, Y., Keller, L., Smith, G. D.,
606 Pellicer, A., Scott, R. T., Jr., Seli, E., & Zernicka-Goetz, M. (2020). Developmental potential of
607 aneuploid human embryos cultured beyond implantation. *Nat Commun*, *11*(1), 3987.
608 https://doi.org/10.1038/s41467-020-17764-7
609 Simoes-Sousa, S., Littler, S., Thompson, S. L., Minshall, P., Whalley, H., Bakker, B., Belkot, K., Moralli,
610 D., Bronder, D., Tighe, A., Spierings, D. C. J., Bah, N., Graham, J., Nelson, L., Green, C. M.,
611 Foijer, F., Townsend, P. A., & Taylor, S. S. (2018). The p38alpha Stress Kinase Suppresses
612 Aneuploidy Tolerance by Inhibiting Hif-1alpha. *Cell Rep*, *25*(3), 749-760 e746.
613 https://doi.org/10.1016/j.celrep.2018.09.060
614 Singla, S., Iwamoto-Stohl, L. K., Zhu, M., & Zernicka-Goetz, M. (2020). Autophagy-mediated apoptosis
615 eliminates aneuploid cells in a mouse model of chromosome mosaicism. *Nat Commun*, *11*(1),
616 2958. https://doi.org/10.1038/s41467-020-16796-3
617 Soto, M., Raaijmakers, J. A., Bakker, B., Spierings, D. C. J., Lansdorp, P. M., Foijer, F., & Medema, R. H.
618 (2017). p53 Prohibits Propagation of Chromosome Segregation Errors that Produce Structural
619 Aneuploidies. *Cell Rep*, *19*(12), 2423-2431. https://doi.org/10.1016/j.celrep.2017.05.055
620 Starostik, M. R., Sosina, O. A., & McCoy, R. C. (2020). Single-cell analysis of human embryos reveals
621 diverse patterns of aneuploidy and mosaicism. *Genome Res*, *30*(6), 814-825.
622 https://doi.org/10.1101/gr.262774.120
623 Thompson, S. L., & Compton, D. A. (2010). Proliferation of aneuploid human cells is limited by a p53-
624 dependent mechanism. *J Cell Biol*, *188*(3), 369-381. https://doi.org/10.1083/jcb.200905057
625 Vanneste, E., Voet, T., Le Caignec, C., Ampe, M., Konings, P., Melotte, C., Debrock, S., Amyere, M.,
626 Vikkula, M., Schuit, F., Fryns, J. P., Verbeke, G., D'Hooghe, T., Moreau, Y., & Vermeesch, J. R.
627 (2009). Chromosome instability is common in human cleavage-stage embryos. *Nat Med*, *15*(5),
628 577-583. https://doi.org/10.1038/nm.1924
629 Vazquez-Diez, C., Paim, L. M. G., & FitzHarris, G. (2019). Cell-Size-Independent Spindle Checkpoint
630 Failure Underlies Chromosome Segregation Error in Mouse Embryos. *Curr Biol*, *29*(5), 865-873
631 e863. https://doi.org/10.1016/j.cub.2018.12.042
632 Yang, M., Rito, T., Metzger, J., Naftaly, J., Soman, R., Hu, J., Albertini, D. F., Barad, D. H., Brivanlou, A.
633 H., & Gleicher, N. (2021). Depletion of aneuploid cells in human embryos and gastruloids. *Nat*
634 *Cell Biol*, *23*(4), 314-321. https://doi.org/10.1038/s41556-021-00660-7
635 Zhao, T., Ren, H., Jia, L., Chen, J., Xin, W., Yan, F., Li, J., Wang, X., Gao, S., Qian, D., Huang, C., &
636 Hao, J. (2015). Inhibition of HIF-1alpha by PX-478 enhances the anti-tumor effect of gemcitabine

637 by inducing immunogenic cell death in pancreatic ductal adenocarcinoma. *Oncotarget*, *6*(4),
638 2250-2262. https://doi.org/10.18632/oncotarget.2948
639 Zhu, J., Tsai, H. J., Gordon, M. R., & Li, R. (2018). Cellular Stress Associated with Aneuploidy. *Dev Cell*,
640 *44*(4), 420-431. https://doi.org/10.1016/j.devcel.2018.02.002
641 Zhu, M., Shahbazi, M., Martin, A., Zhang, C., Sozen, B., Borsos, M., Mandelbaum, R. S., Paulson, R. J.,
642 Mole, M. A., Esbert, M., Titus, S., Scott, R. T., Campbell, A., Fishel, S., Gradinaru, V., Zhao, H.,
643 Wu, K., Chen, Z. J., Seli, E., . . . Zernicka Goetz, M. (2021). Human embryo polarization requires
644 PLC signaling to mediate trophectoderm specification. *Elife*, *10*.
645 https://doi.org/10.7554/eLife.65068
646 Zhu, M., & Zernicka-Goetz, M. (2020). Principles of Self-Organization of the Mammalian Embryo. *Cell*,
647 *183*(6), 1467-1478. https://doi.org/10.1016/j.cell.2020.11.003
648

649 **FIGURES AND FIGURE LEGENDS**

650 Figure 1| **Lineage analysis of aneuploid embryos generated by selective Mps1 inhibitors AZ3146 and**
651 **reversine.**

652 (A) Graphic representation of 4-cell embryos treated with DMSO (control) or Mps1 inhibitors reversine (0.5
653 μM) and AZ3146 (20 μM) to inactivate the spindle assembly checkpoint (SAC) and induce chromosome
654 segregation errors. After washing, embryos were cultured to the mature blastocyst stage (E4.5) and
655 analyzed for lineage specification. (B) Immunofluorescence imaging of well-known lineage markers CDX2
656 (TE), NANOG (EPI) and SOX17 (PE) reveals that overall embryonic morphology and cavitation is not
657 affected by Mps1 inhibition. (C) Number of cells in each lineage was quantified to evaluate the effect of
658 drug treatment on blastocyst development. Importantly, both reversine and AZ3146-treatments reduce the
659 number of cells in the ICM, marked by NANOG (EPI) and SOX17 (PE). Whereas the TE, marked by CDX2,
660 is reduced only in the reversine-treated embryos. (n=28 embryos per treatment, cumulative of three
661 independent experiments. Statistical test: Mann–Whitney U-test, error bars represent s.e.m). (D) Analysis
662 of DNA damage and DNA repair based on immunofluorescence against γH2A.X (phosphorylated form of
663 H2A.X, white) and PARP1 (red), respectively. (E) Intensity analysis shows that reversine and AZ3146
664 increase DNA damage at the 8-cell stage through morula stage compared with DMSO-treated embryos.
665 Importantly, reversine appears to downregulate PARP1 expression at the 8-cell stage, which extends to
666 morula stage embryos (n=~15 embryos per treatment, ~120 cells. Collection was made during three
667 independent experiments Statistical test: t-test, error bars represent s.e.m).
668

669 Figure 2 | **AZ3146-treated embryos elevate HIF1A activity to support formation of the TE and PE.**

670 A) qPCR analysis of *p53* and *Hif1a* mRNA expression at morula and blastocyst stages reveals that *p53* is
671 upregulated in reversine-treated embryos and that *Hif1a* is upregulated in AZ3146-treated embryos at
672 morula stages (Sample: three biological replicates and two technical replicates per experiment with each
673 replicate having a minimum of 16 embryos. Statistical test: Welch's t-test). B) Immunofluorescence against
674 HIF1A (black) shows an increase in nuclear intensity in AZ3146-treated embryos at morula stages. At
675 blastocyst stage, nuclear and cytoplasmic HIF1A are increased in AZ3146-treated embryos; normalization
676 was based on DAPI staining (magenta). (n=~20embryos per treatment. Statistical test: Mann–Whitney U-
677 test, error bars represent s.e.m) (C) Graphic representation of 4-cell embryos treated with DMSO and

678 aneuploid drugs. Downregulation of HIF1A was achieved by treatment with IDF-11774 immediately after
679 wash of the aneuploid drugs. Immunofluorescence analysis of lineage specification in blastocyst cultured
680 with the HIF1A inhibitor IDF-11774 using antibodies against CDX2 (TE), NANOG (EPI) and SOX17 (PE).
681 Importantly, IDF-11774 appears to affect cavitation of some AZ3146-treated embryos. (D) Lineage analysis
682 at the blastocyst stage shows that TE and PE specification are affected by IDF-11774 treatment. Number
683 of cells in each lineage was quantified to evaluate the effect on blastocyst development (n=20 embryos per
684 treatment collected from three independent experiments. Statistical test: Mann–Whitney U-test, error bars
685 represent s.e.m.).
686
687 Figure 3 | **Hypoxia exposure reduces DNA damage and affects lineage proportions in the aneuploid**
688 **blastocyst.**
689 (A) Graphic representation of the hypoxia experiments. 2-cell embryos were cultured until the blastocyst
690 stage in hypoxia conditions (5% oxygen). As before, 4-cell stage embryos were treated with DMSO or Mps1
691 inhibitors reversine and AZ3146 until the 8-cell stage. After washing, embryos were cultured to the mature
692 blastocyst stage (E4.5) and analyzed for lineage specification. (B) Immunofluorescence imaging of well-
693 known lineage markers CDX2 (TE), NANOG (EPI) and SOX17 (PE) reveals that overall embryonic
694 morphology and cavitation is not affected by Mps1 inhibition or hypoxia. (C) Lineage analysis at blastocyst
695 stage. Number of cells in each lineage was used to evaluate the effects in blastocyst development (n=18
696 embryos per treatment collected from three independent experiments. Statistical test: Mann–Whitney U-
697 test, error bars represent s.e.m,). (D) Immunofluorescence against PARP1 (red) and γH2A.X (white) in
698 blastocyst after drug treatments. (E) Intensity analysis shows that, under hypoxia, at 8-cell stage, DNA
699 damage is increased after exposure to reversine but not AZ3146. PARP1 expression is altered only at the
700 8-cell stage in reversine-treated embryos (n=25 embryos per treatment collected from three independent
701 experiments. Statistical test: t-test, error bars represent s.e.m.).
702
703 Figure 4 | **Hypoxia affects cell competition between diploid and aneuploid cells during pre-**
704 **implantation development.** (A) Graphic representation of the cell competition experiments. Embryos were
705 treated at the 4-cell stage with DMSO or Mps1 inhibitors reversine and AZ3146. After washing, 8-cell stage
706 embryos were disaggregated, and re-aggregated to form chimeras containing a 1:1 ratio of DMSO/AZ314-
707 treated blastomeres and Reversine/AZ314-treated blastomeres. Following aggregation, chimeras were
708 cultured to the mature blastocyst stage (E4.5) and analyzed for lineage specification. For identification of
709 the treatment, we use transgenics lines with membrane markers. Immunofluorescence for CDX2, NANOG,
710 and SOX17 was performed to test lineage specification and allocation during (B) normoxia and (C) hypoxia.
711 Lineage allocation quantification was based on the above markers. Importantly, (D) in normoxia, both
712 chimeras have the same number of cells in all the lineages except the EPI. In addition, AZ3146-treated
713 blastomeres outcompete reversine-treated blastomeres in medium-grade mosaics in the TE and the EPI.
714 (E) Under hypoxia, both chimeras have similar number of cells in all the lineages. Yet, AZ3146-blastomeres

715 do not outcompete reversine-treated blastomeres. Quantification of the contribution of AZ3146-treated
716 blastomeres to the chimeras showed that, (F) under normoxia, compare with DMSO-treated cells, no
717 preferential allocation of aneuploid cells occurs in the TE. In contrast, AZ3146-treated blastomeres
718 increased their contribution when compare with reversine- treated blastomeres, but only for the EPI and
719 the PE. (G) During hypoxia, in DMSO/AZ3146 chimeras no preferential allocation of aneuploid cells occurs
720 in the TE. But preferential allocation of diploid cells to the EPI is observed. Whereas in Reversine/AZ3146
721 chimeras, AZ3146-treated blastomeres contribute similarly to reversine-blastomeres to the TE and PE but
722 significantly increase contribution to the EPI. These results indicate that hypoxia favors the survival of
723 reversine-induced aneuploid cells compared to their survival in normoxia(n>7 embryos per treatment
724 collected from three independent experiments. Statistical test: Mann–Whitney U-test, error bars represent
725 s.e.m).
726
727 Figure 5| **HIF1A inhibition increases the proportion of euploid cells in mosaic embryos.** (A) Schematic
728 of HIF1A inhibition by IDF-11774 in 8-cell stage aggregation chimeras cultured in hypoxia.
729 Immunofluorescence for CDX2, NANOG, and SOX17 was performed to test lineage specification and
730 allocation. (B) HIF1A inhibition in low-grade mosaicism does not affect overall morphology but affects (C)
731 cavity diameter. In addition, (D) lineage allocation quantification reveals a significant reduction of total cell
732 number, as well as a reduction in cell number in the TE but not in the EPI and PE. In contrast, (E) HIF1A
733 inhibition in medium-grade mosaicism affects morphology, and (F) cavitation of the mosaic embryos.
734 However, lineage allocation quantification revealed that total cell number is not affected (G) in medium-
735 grade mosaicism after IDF11-774 treatment. Nevertheless, HIF1A inhibition appears to increase the cell
736 number of the PE. These results show that HIF1A inhibition in hypoxic conditions differentially affect each
737 type of mosaic embryos. (n>8 embryos per treatment collected from three independent experiments.
738 Statistical test: Mann–Whitney U-test, error bars represent s.e.m).
739
740 Figure S.1| **AZ3146-treated embryos are aneuploid and can develop to post-implantation stages.**
741 (A) *In situ* chromosome counting of 8-cell stage embryos after drug treatments. Representative images of
742 individual embryos in the different treatments. DNA (white) is visualized by DAPI staining and kinetochores
743 (red) by CREST antibody. PB (polar body), MN (micronuclei). Each chromosome presents 2 CREST dots.
744 The large number is the cell ID and the smaller number indicates the number of chromosomes, “n”. Diploid
745 blastomeres present 40 pairs of CREST dots. Phalloidin (cyan) was used for cell segmentation. (B)
746 Quantification of the incidence of aneuploid events, designated as those with more than 2 chromosomes
747 (MN>2chr), less than 2 chromosomes (MN<2chr), without kinetochores (MN-CREST) and non-dividing
748 nucleus (ND cell). We observed an increase in MN following reversine and AZ3146 treatment. Importantly,
749 reversine-treated cells have a higher number of ND cells and MN-CREST staining. (n=256 cell DMSO
750 treatment, n=304 cells AZ3146 treatment, n=144 cells reversine treatment, n=~20 embryos per treatment.
751 Statistical test: Mann–Whitney U-test, error bars represent s.e.m). (C) Embryo transfer experiments show

752 higher implantation events (% decidua formation) in AZ3146-treated embryos. The left uterine horn was
753 used for transfer of reversine-treated blastocyst and the right uterine horn for AZ3146-treated blastocyst.
754 (n=7 embryos transplanted per uterine horn, repeated experiments two times) (D) Only AZ3146-treated
755 blastocyst can develop post-gastrulation E9.5 fetuses, image representing three out of five surviving
756 embryos (% embryo formation).
757
758 Figure S.2| **PARP1 is required for ICM development**.
759 (A) Immunofluorescence against PARP1 (red) and γH2A.X (white) in blastocyst after drug treatments.
760 Notice accumulation of DNA damage in reversine-treated blastocyst (Representative images of n>12
761 embryos per treatment collected from three independent experiments). (B) Immunofluorescence against
762 PARP1 (red), NANOG (white, epiblast) and CDX2 (green, trophectoderm) at the blastocyst stage in
763 untreated embryos. Analysis of PARP1 intensity shows an increase in the EPI lineage (n>21 embryos per
764 treatment collected from three independent experiments. Statistical test: Mann–Whitney U-test, error bars
765 represent s.e.m,). To confirm these observation, scRNA-seq (Deng et. al 2014) shows enrichment of *Parp1*
766 mRNA specifically in the EPI. (C) Graphic representation of 4-cell embryos treated with DMSO and
767 aneuploid drugs. Downregulation of PARP1 was achieved by treatment with Olaparib from morula to
768 blastocyst stage. (D) Effects of the inhibition of PARP1 function were assessed by immunofluorescence
769 against CDX2 (TE), NANOG (EPI) and SOX17 (PE) in the different treatments. Importantly, Olaparib
770 treatment does not affect blastocyst morphology. (E) Lineage analysis at blastocyst stage shows a specific
771 effect on the survival of epiblast and PE cells in reversine-treated embryos. Ratio of cells in each lineage
772 in the blastocyst is normalized based on DMSO treatment (n=15 embryos per treatment collected from
773 three independent experiments. Statistical test: Mann–Whitney U-test, error bars represent s.e.m).
774
775 Figure S.3| **Pharmacological inhibitors of HIF1A have distinct effects on mouse pre-implantation**
776 **embryos.** (A) Inhibition of HIF1A from zygotes to blastocyst stage with PX-478 or IDF-11774 in normoxia.
777 Immunofluorescence against CDX2 (TE) and DAPI (magenta) was used to assess blastocyst development.
778 Importantly, IDF-11774 does not compromise pre-implantation development, whereas PX-478
779 compromised the survival and overall morphology of the blastocyst. (B) Analysis of the number of
780 trophectoderm cells (CDX2) and total number (DAPI) shows a deleterious effect of PX-478 during blastocyst
781 development (n=~12 embryos per treatment collected from three independent experiments. Statistical test:
782 Mann–Whitney U-test, error bars represent s.e.m).
783
784 Figure S.4| **Correlation plot of AZ3146-treated cells in the epiblast and trophectoderm.** Scatter plot of
785 AZ3146-treated cells in epiblast and trophectoderm in DMSO/AZ3146 and Reversine/AZ3146 mosaic
786 blastocysts cultured under normoxic and hypoxic conditions.
787

788 Figure S.5| **Aneuploidies generated before the 2-cell stage does not affect lineage specification in**
789 **mosaic embryos.** (A) Immunofluorescence for CDX2, NANOG, and SOX17 was performed in blastocysts
790 after zygote treatment with Mps1 inhibitors. Importantly, reversine treatment at zygote stages affects
791 morphology of blastocyst. (B) Lineage analysis of blastocyst shows no effect in AZ3146-treated embryos.
792 Whereas reversine treatment reduces the cell number to almost half. Ratio of cells in each lineage in the
793 blastocyst is normalized based on DMSO treatments. (n=~27 embryos per treatment collected from three
794 independent experiments. Statistical test: Mann–Whitney U-test, error bars represent s.e.m). (C)
795 Aggregation chimeras at 2-cell stage were created by using transgenics lines with membrane markers:
796 mTmG (green) and E-cadherin (white). Subsequently, (D) immunofluorescence for CDX2, NANOG, and
797 SOX17 was performed to quantify lineage allocation. Our results show no effect on embryo morphology in
798 our chimeras. However, reversine/DMSO (D/R) chimeras seems to have increase events of cell extrusion
799 and reversine/AZ3146 chimeras are smaller in number of cells compare with DMSO/AZ3146 chimeras. (E)
800 Data show the proportion of AZ3146-treated cells in DMSO/AZ3146 mosaic blastocysts (grey) and in
801 reversine/AZ3146 mosaic blastocysts (blue), as well as the proportion of reversine-treated cells in
802 DMSO/reversine mosaic blastocysts (red).
803
804 Figure S.6| **IDF-11774-mediated inhibition of HIF1A increases the proportion of euploid cells in**
805 **mosaic embryos.** Brightfield images of low- and medium-mosaic chimeras grown in normoxia and treated
806 with (A) DMSO and (B) IDF-11774. Quantification of the contribution of AZ3146-treated blastomeres to the
807 chimeras showed that, (C) in DMSO/AZ3146 mosaics, IDF-11774 treatment reduces the proportion of
808 AZ3146-treated blastomeres, whereas (D) in reversine/AZ3146 mosaics, IDF-11774 treatment slightly
809 increases the proportion of AZ3146-treated blastomeres. These results may indicate that HIF1A inhibition
810 impairs the less fit population in chimeric embryos.
811

Figure 1

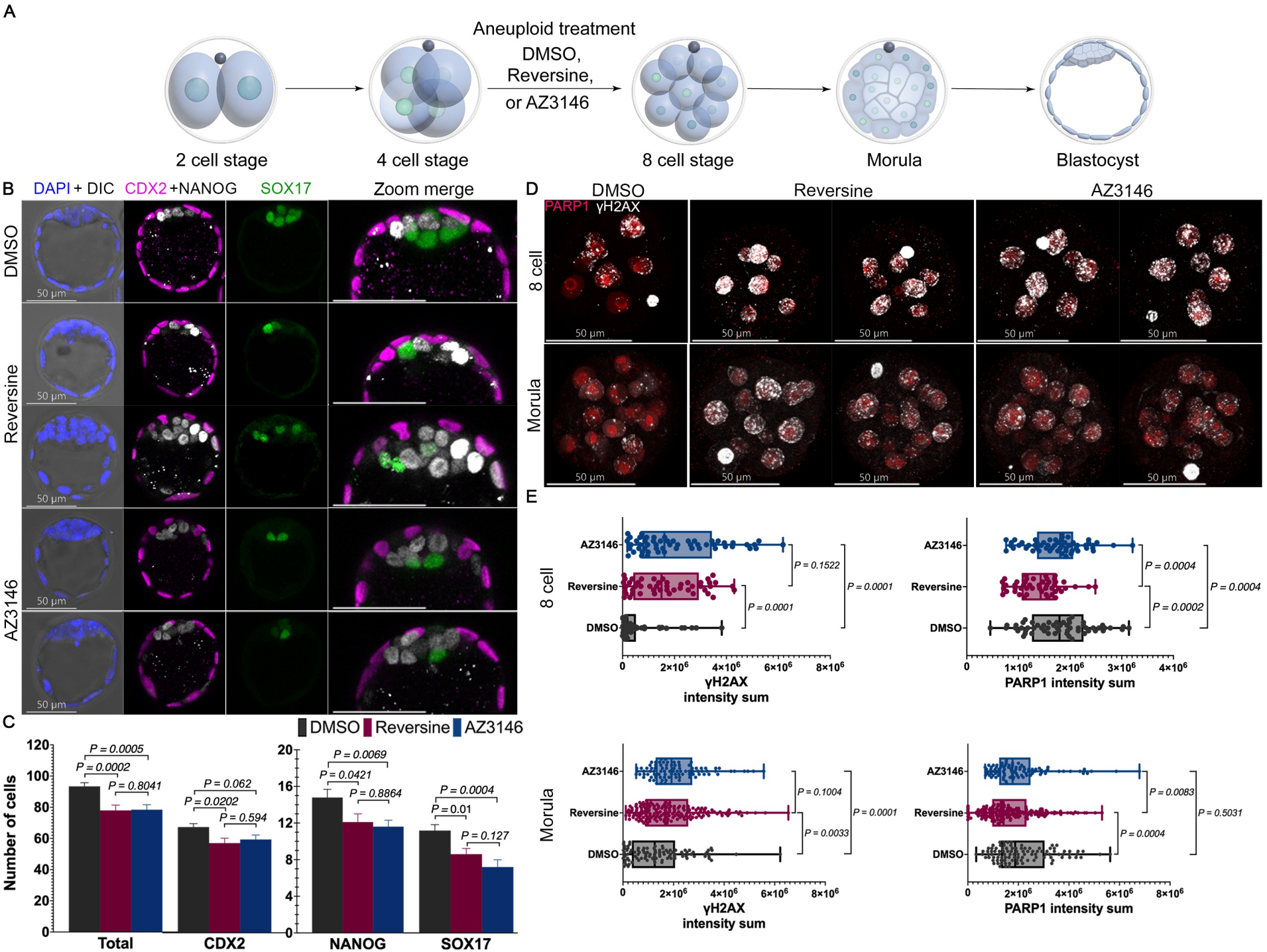
A
Aneuploid treatment
DMSO,
Reversine,
or AZ3146
2 cell stage
4 cell stage
8 cell stage
Morula
Blastocyst
B
DAPI + DIC
CDX2 +NANOG
SOX17
Zoom merge
DMSO
Reversine
AZ3146
50 µm
C
DMSO
Reversine
AZ3146
Number of cells
P = 0.0005
P = 0.0002
P = 0.8041
P = 0.062
P = 0.0202
P = 0.594
P = 0.0069
P = 0.0421
P = 0.8864
P = 0.0004
P = 0.01
P = 0.127
Total
CDX2
NANOG
SOX17
D
DMSO
Reversine
AZ3146
PARP1 γH2AX
8 cell
Morula
50 µm
E
8 cell
Morula
AZ3146
Reversine
DMSO
P = 0.1522
P = 0.0001
P = 0.0001
P = 0.0004
P = 0.0004
P = 0.0002
P = 0.1004
P = 0.0001
P = 0.0033
P = 0.0083
P = 0.5031
P = 0.0004
γH2AX
intensity sum
PARP1 intensity sum

Figure 2

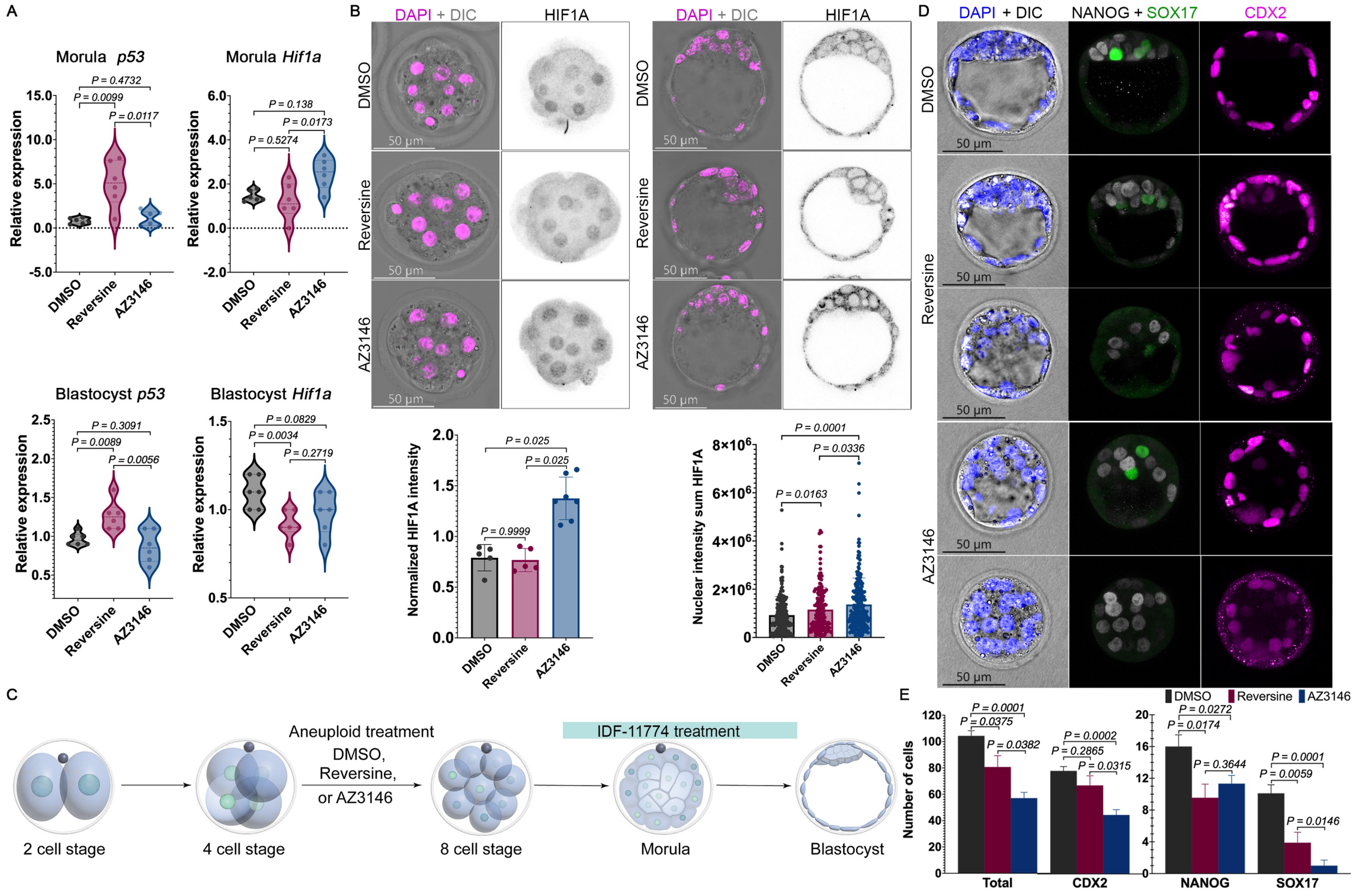
A
Morula p53
Morula Hif1a
Blastocyst p53
Blastocyst Hif1a
Relative expression
P = 0.4732
P = 0.0099
P = 0.0117
P = 0.138
P = 0.0173
P = 0.5274
P = 0.3091
P = 0.0089
P = 0.0056
P = 0.0829
P = 0.0034
P = 0.2719
DMSO
Reversine
AZ3146
B
DAPI + DIC
HIF1A
50 µm
Normalized HIF1A intensity
P = 0.025
P = 0.025
P = 0.9999
Nuclear intensity sum HIF1A
P = 0.0001
P = 0.0336
P = 0.0163
C
Aneuploid treatment
DMSO,
Reversine,
or AZ3146
IDF-11774 treatment
2 cell stage
4 cell stage
8 cell stage
Morula
Blastocyst
D
DAPI + DIC
NANOG + SOX17
CDX2
E
Number of cells
Total
CDX2
NANOG
SOX17
P = 0.0001
P = 0.0375
P = 0.0382
P = 0.0002
P = 0.2865
P = 0.0315
P = 0.0272
P = 0.0174
P = 0.3644
P = 0.0001
P = 0.0059
P = 0.0146

Figure 3

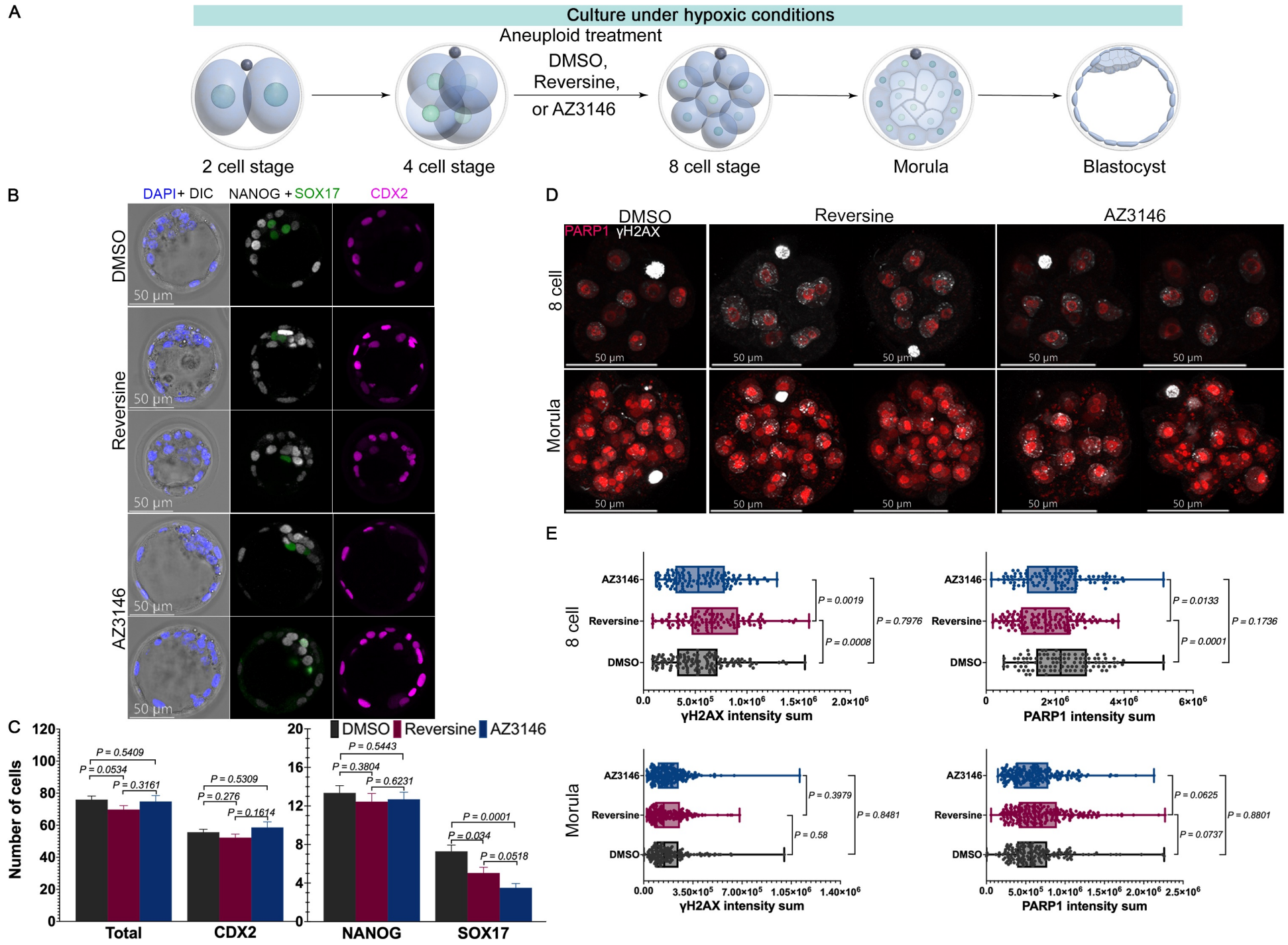
A
Culture under hypoxic conditions
Aneuploid treatment
DMSO,
Reversine,
or AZ3146
2 cell stage
4 cell stage
8 cell stage
Morula
Blastocyst
B
DAPI+ DIC
NANOG + SOX17
CDX2
DMSO
Reversine
AZ3146
50 µm
C
DMSO
Reversine
AZ3146
Number of cells
Total
CDX2
NANOG
SOX17
P = 0.5409
P = 0.0534
P = 0.3161
P = 0.5309
P = 0.276
P = 0.1614
P = 0.5443
P = 0.3804
P = 0.6231
P = 0.0001
P = 0.034
P = 0.0518
D
DMSO
Reversine
AZ3146
PARP1 γH2AX
8 cell
Morula
50 µm
E
8 cell
Morula
AZ3146
Reversine
DMSO
P = 0.0019
P = 0.0008
P = 0.7976
P = 0.0133
P = 0.0001
P = 0.1736
P = 0.3979
P = 0.58
P = 0.8481
P = 0.0625
P = 0.0737
P = 0.8801
γH2AX intensity sum
PARP1 intensity sum

Figure 4

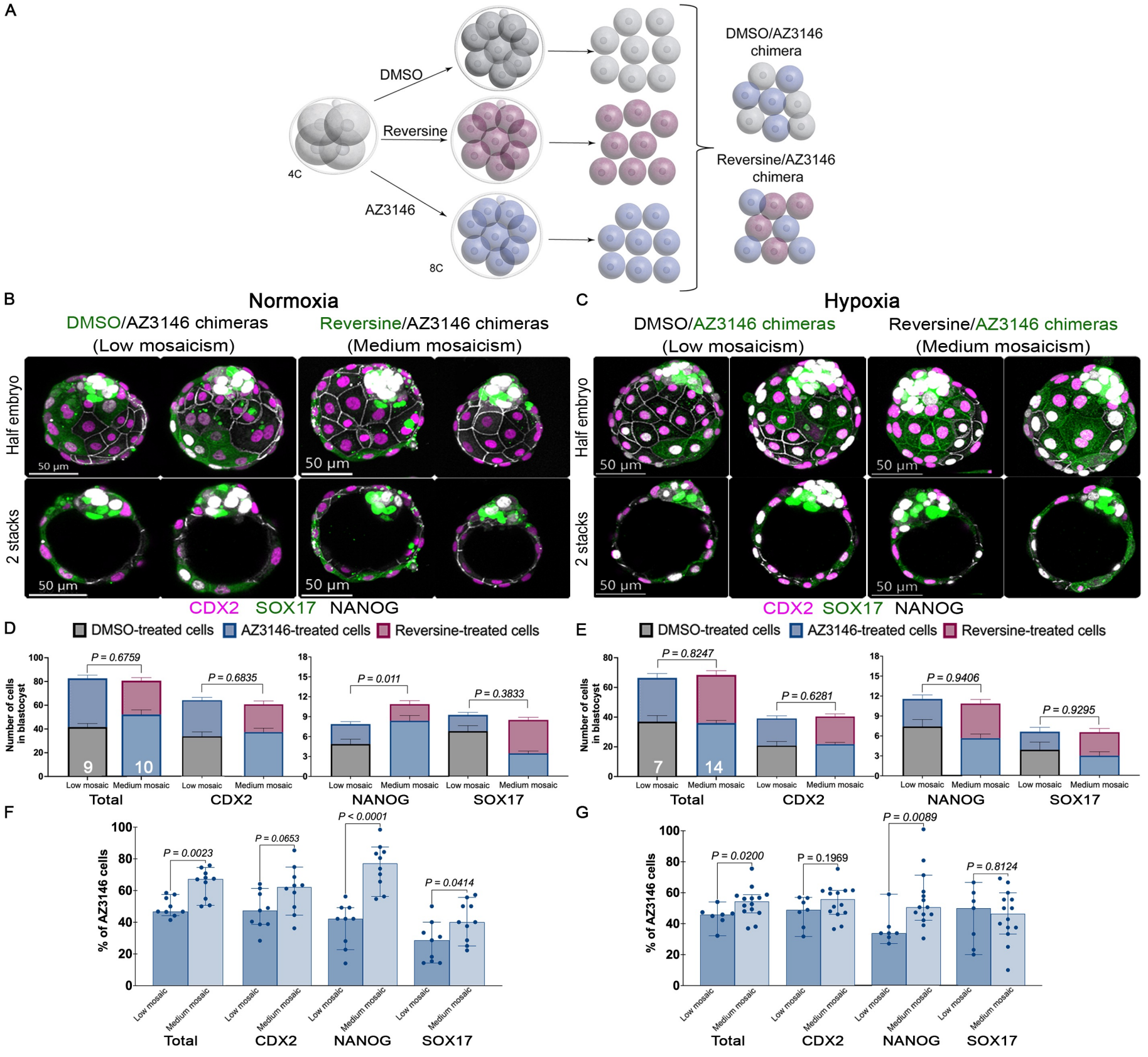
A
DMSO
Reversine
AZ3146
4C
8C
DMSO/AZ3146 chimera
Reversine/AZ3146 chimera
B
Normoxia
DMSO/AZ3146 chimeras (Low mosaicism)
Reversine/AZ3146 chimeras (Medium mosaicism)
Half embryo
2 stacks
50 µm
CDX2 SOX17 NANOG
C
Hypoxia
DMSO/AZ3146 chimeras (Low mosaicism)
Reversine/AZ3146 chimeras (Medium mosaicism)
Half embryo
2 stacks
50 µm
CDX2 SOX17 NANOG
D
DMSO-treated cells
AZ3146-treated cells
Reversine-treated cells
Number of cells in blastocyst
P = 0.6759
P = 0.6835
P = 0.011
P = 0.3833
9
10
Low mosaic
Medium mosaic
Total
CDX2
NANOG
SOX17
E
DMSO-treated cells
AZ3146-treated cells
Reversine-treated cells
Number of cells in blastocyst
P = 0.8247
P = 0.6281
P = 0.9406
P = 0.9295
7
14
Low mosaic
Medium mosaic
Total
CDX2
NANOG
SOX17
F
% of AZ3146 cells
P = 0.0023
P = 0.0653
P < 0.0001
P = 0.0414
Low mosaic
Medium mosaic
Total
CDX2
NANOG
SOX17
G
% of AZ3146 cells
P = 0.0200
P = 0.1969
P = 0.0089
P = 0.8124
Low mosaic
Medium mosaic
Total
CDX2
NANOG
SOX17

Figure 5

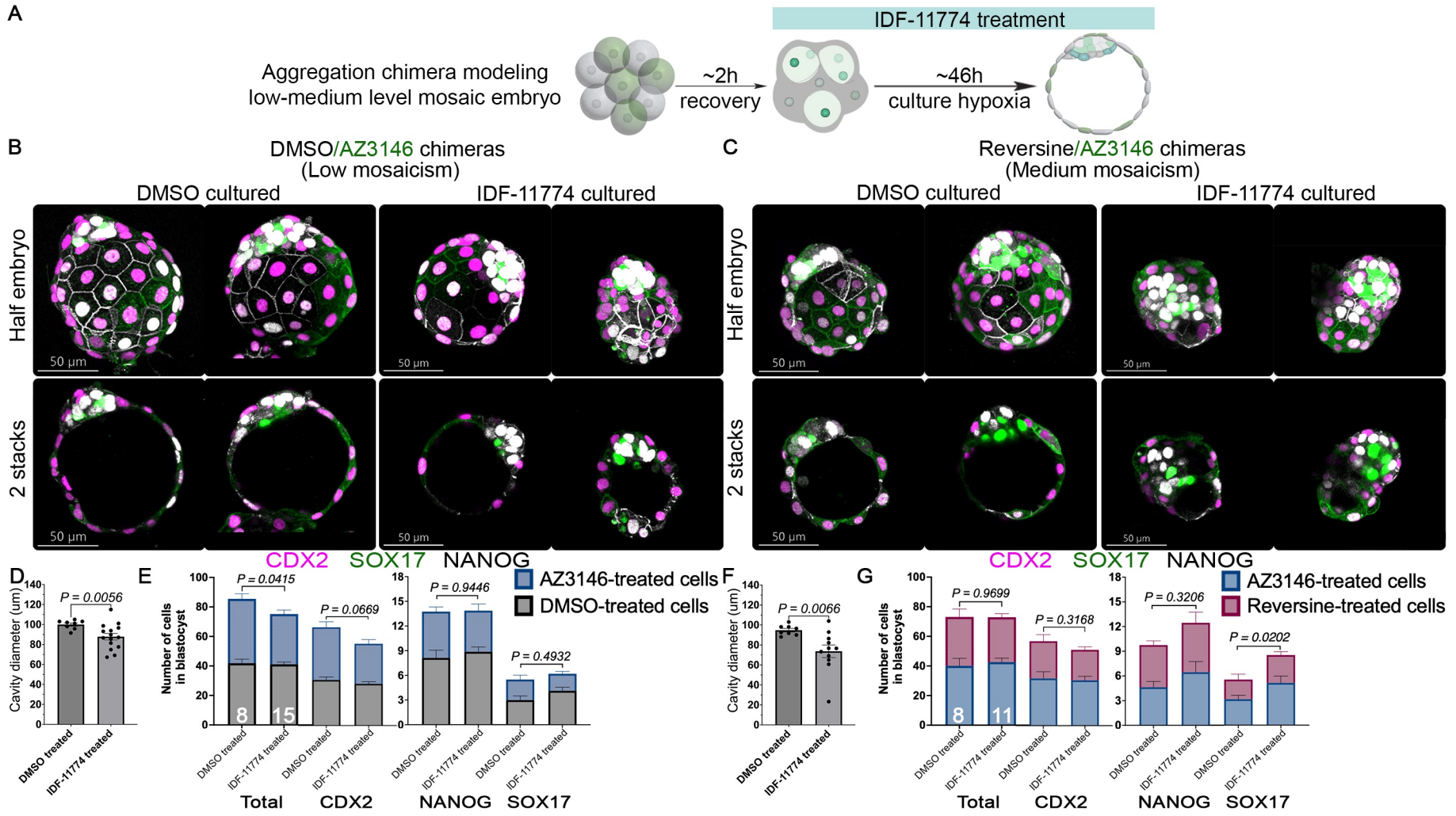
A
IDF-11774 treatment
Aggregation chimera modeling
low-medium level mosaic embryo
~2h
recovery
~46h
culture hypoxia
B
DMSO/AZ3146 chimeras
(Low mosaicism)
DMSO cultured
IDF-11774 cultured
Half embryo
2 stacks
50 µm
C
Reversine/AZ3146 chimeras
(Medium mosaicism)
DMSO cultured
IDF-11774 cultured
Half embryo
2 stacks
50 µm
D
Cavity diameter (um)
P = 0.0056
DMSO treated
IDF-11774 treated
E
CDX2 SOX17 NANOG
Number of cells in blastocyst
P = 0.0415
P = 0.0669
P = 0.9446
P = 0.4932
8
15
AZ3146-treated cells
DMSO-treated cells
DMSO treated
IDF-11774 treated
Total
CDX2
NANOG
SOX17
F
Cavity diameter (um)
P = 0.0066
DMSO treated
IDF-11774 treated
G
CDX2 SOX17 NANOG
Number of cells in blastocyst
P = 0.9699
P = 0.3168
P = 0.3206
P = 0.0202
8
11
AZ3146-treated cells
Reversine-treated cells
DMSO treated
IDF-11774 treated
Total
CDX2
NANOG
SOX17

Figure S. 1

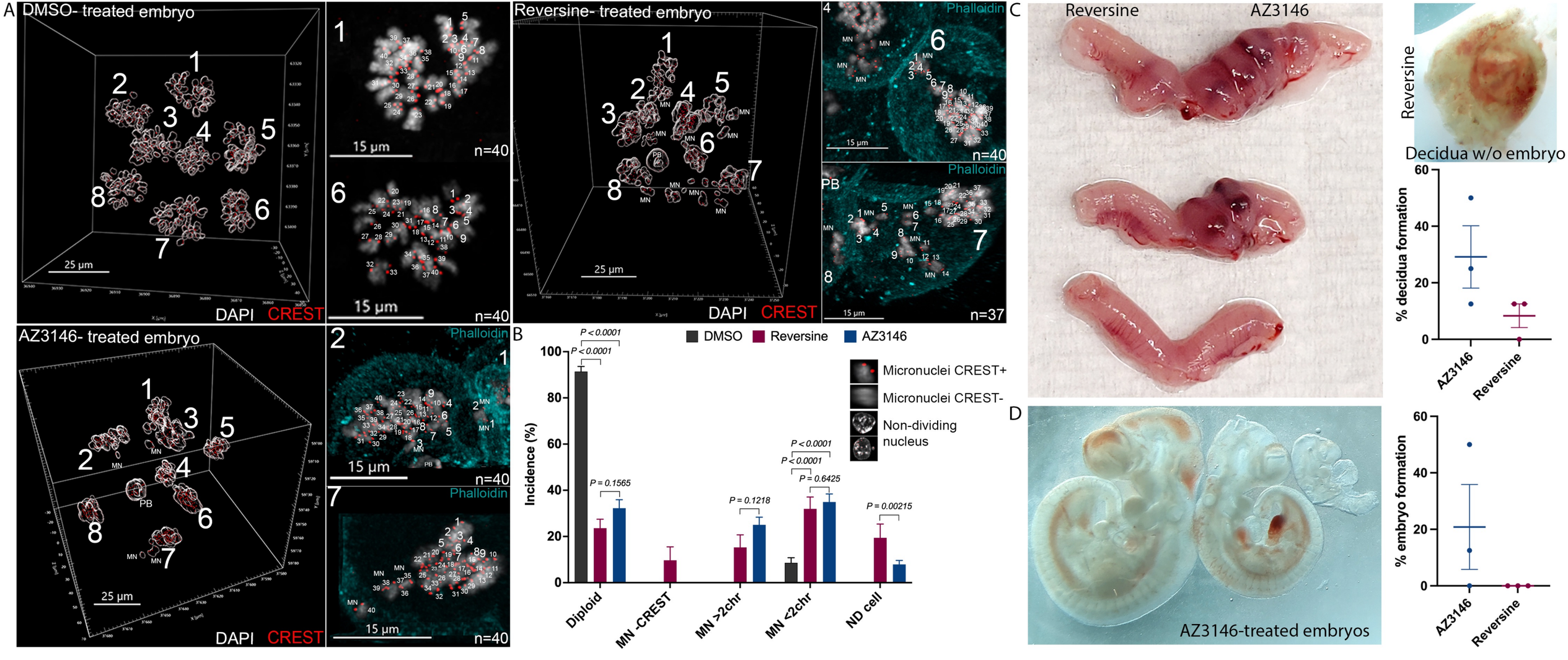
A
DMSO- treated embryo
25 µm
DAPI CREST
15 µm
n=40
Reversine- treated embryo
Phalloidin
n=37
AZ3146- treated embryo
B
DMSO
Reversine
AZ3146
Micronuclei CREST+
Micronuclei CREST-
Non-dividing nucleus
Incidence (%)
P < 0.0001
P = 0.1565
P = 0.1218
P = 0.6425
P = 0.00215
Diploid
MN -CREST
MN >2chr
MN <2chr
ND cell
C
Reversine
AZ3146
Decidua w/o embryo
% decidua formation
D
AZ3146-treated embryos
% embryo formation

Figure S.2

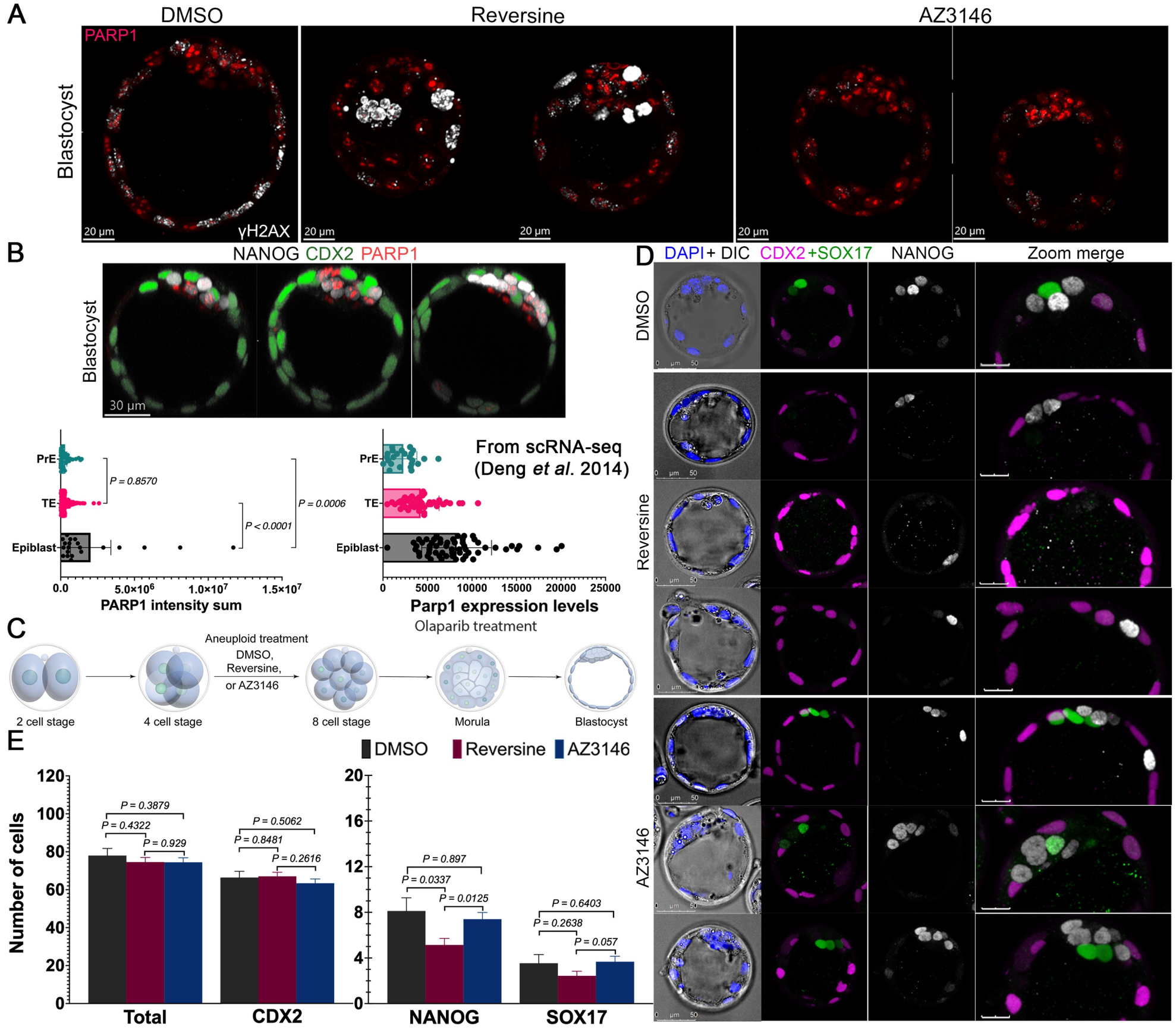
A
DMSO
Reversine
AZ3146
PARP1
Blastocyst
γH2AX
20 µm
B
NANOG CDX2 PARP1
Blastocyst
30 µm
PrE
TE
Epiblast
P = 0.8570
P = 0.0006
P < 0.0001
0.0
5.0×10^6
1.0×10^7
1.5×10^7
PARP1 intensity sum
From scRNA-seq
(Deng et al. 2014)
0
5000
10000
15000
20000
25000
Parp1 expression levels
C
Olaparib treatment
Aneuploid treatment
DMSO,
Reversine,
or AZ3146
2 cell stage
4 cell stage
8 cell stage
Morula
Blastocyst
D
DAPI + DIC
CDX2 +SOX17
NANOG
Zoom merge
DMSO
Reversine
AZ3146
E
DMSO
Reversine
AZ3146
Number of cells
P = 0.3879
P = 0.4322
P = 0.929
P = 0.5062
P = 0.8481
P = 0.2616
P = 0.897
P = 0.0337
P = 0.0125
P = 0.6403
P = 0.2638
P = 0.057
Total
CDX2
NANOG
SOX17

Figure S. 3

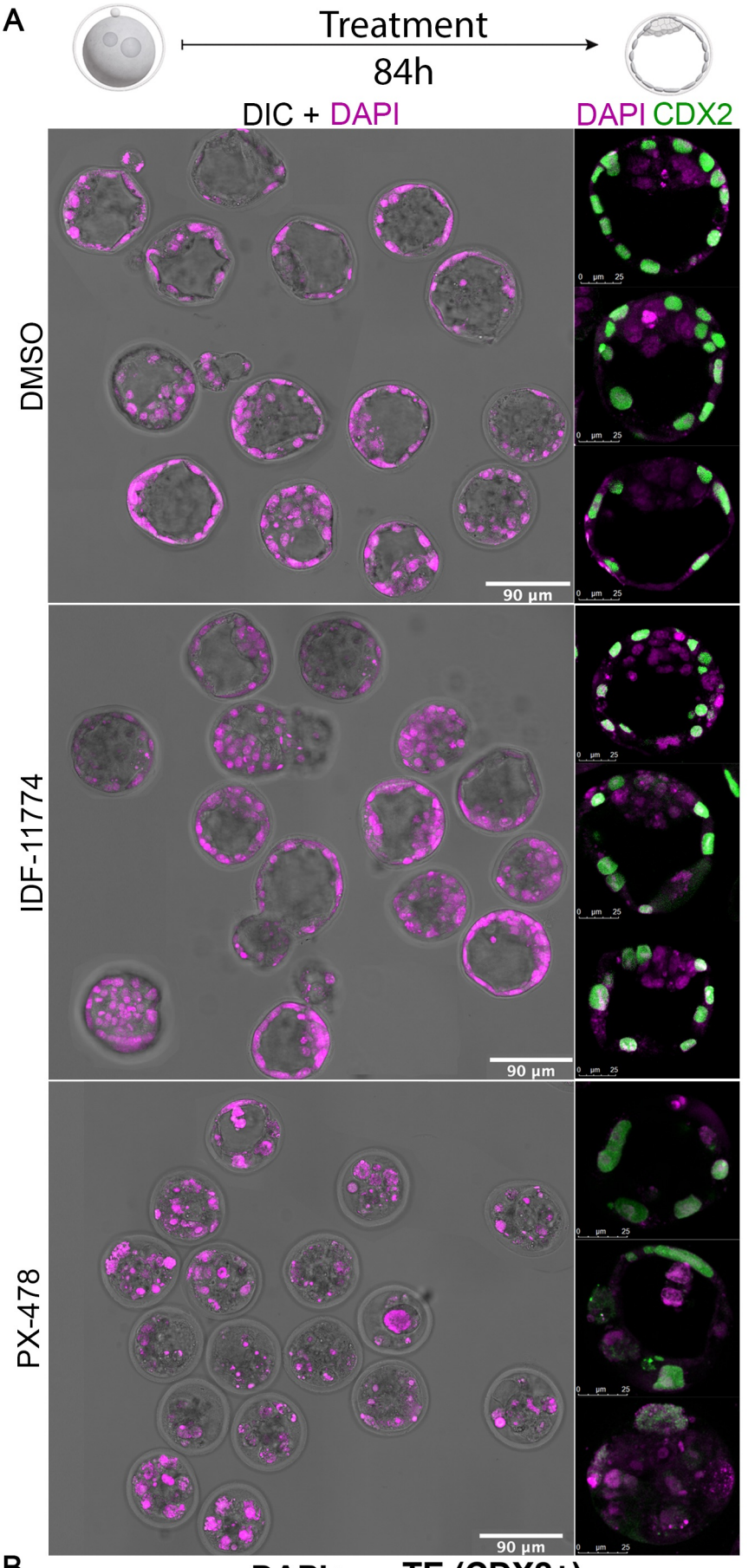
A
Treatment
84h
DIC + DAPI
DAPI CDX2
DMSO
IDF-11774
PX-478
90 µm
90 µm
90 µm

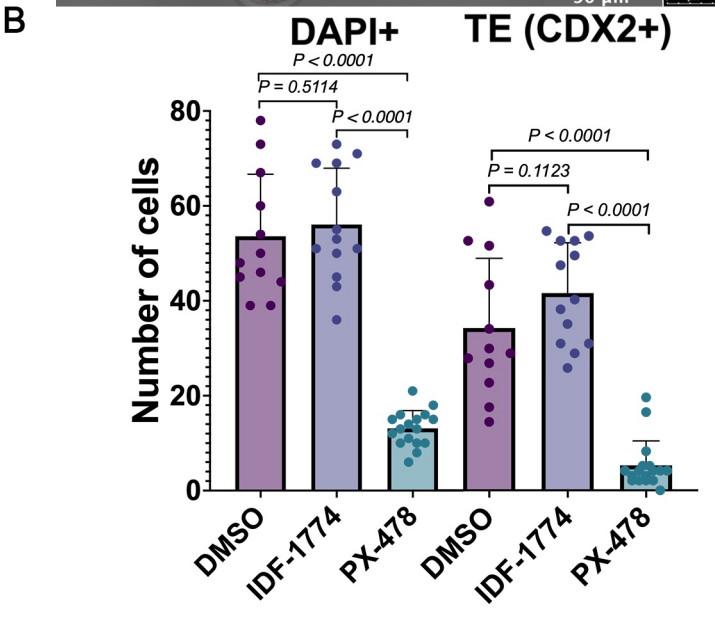
B
DAPI+
TE (CDX2+)
P < 0.0001
P = 0.5114
P < 0.0001
P < 0.0001
P = 0.1123
P < 0.0001
Number of cells
80
60
40
20
0
DMSO
IDF-1774
PX-478
DMSO
IDF-1774
PX-478

Figure S. 4

A

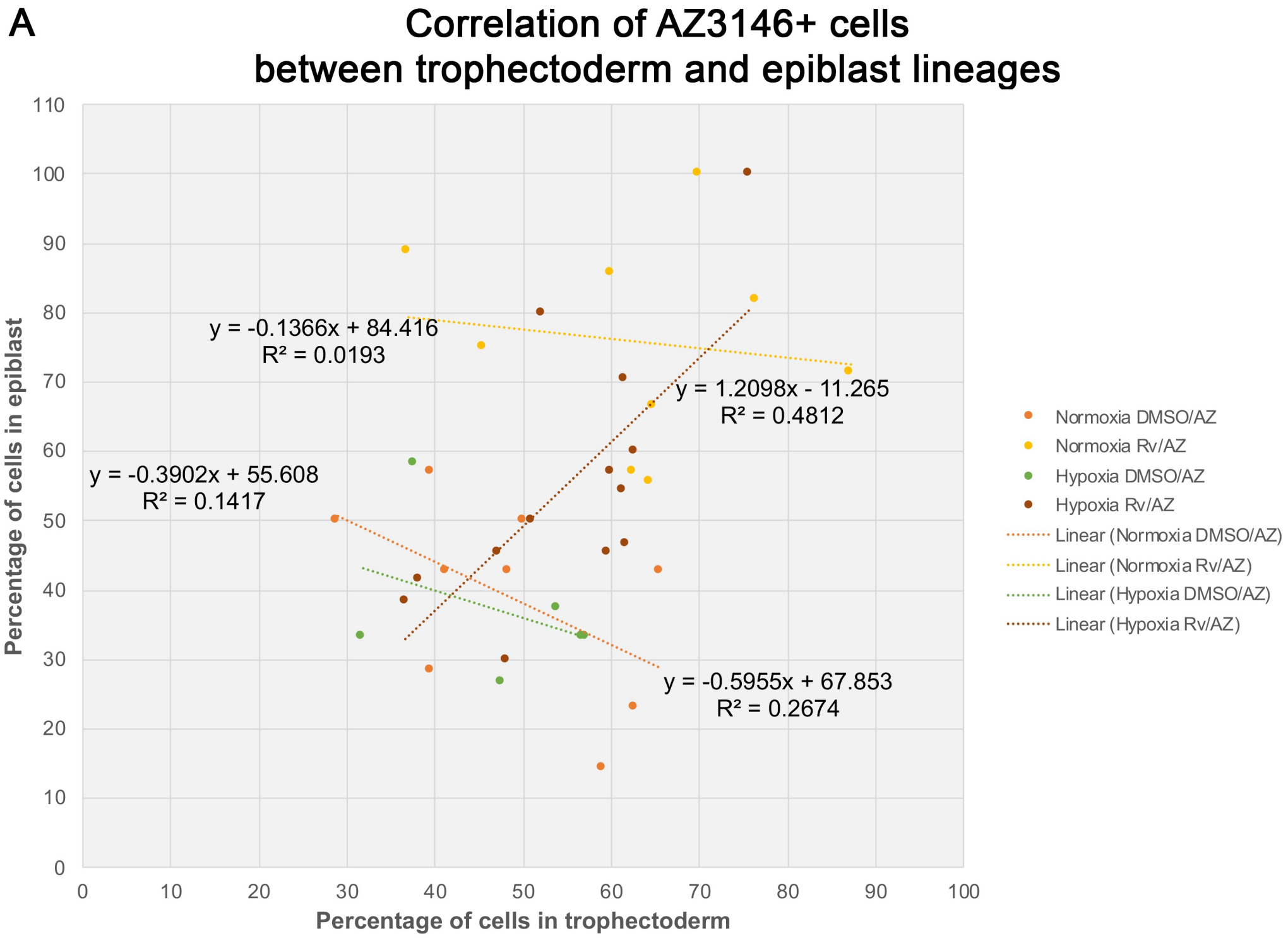
Correlation of AZ3146+ cells
between trophectoderm and epiblast lineages
Percentage of cells in epiblast
Percentage of cells in trophectoderm
0
10
20
30
40
50
60
70
80
90
100
110
y = -0.1366x + 84.416
R² = 0.0193
y = 1.2098x - 11.265
R² = 0.4812
y = -0.3902x + 55.608
R² = 0.1417
y = -0.5955x + 67.853
R² = 0.2674
Normoxia DMSO/AZ
Normoxia Rv/AZ
Hypoxia DMSO/AZ
Hypoxia Rv/AZ
Linear (Normoxia DMSO/AZ)
Linear (Normoxia Rv/AZ)
Linear (Hypoxia DMSO/AZ)
Linear (Hypoxia Rv/AZ)

Figure S. 5

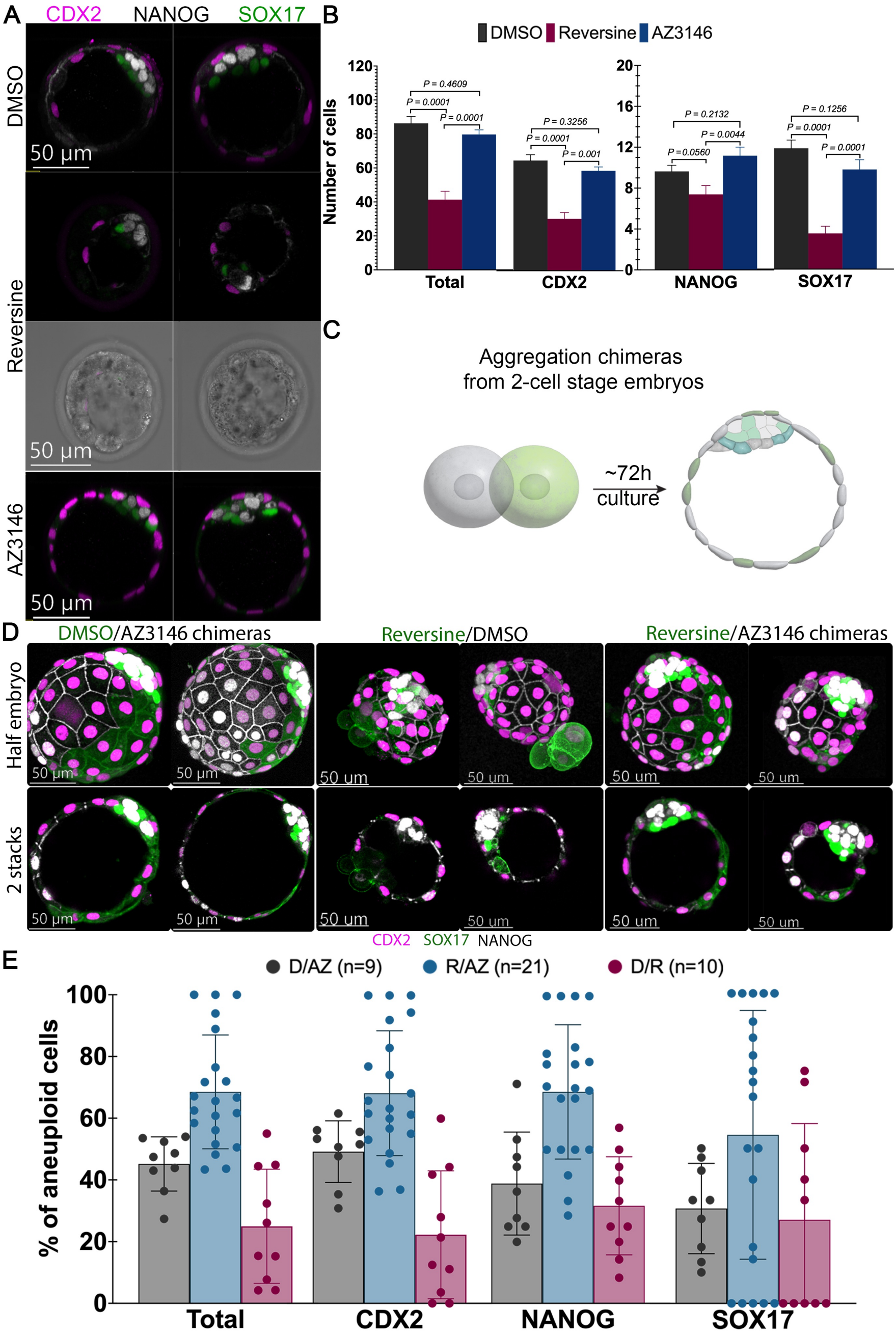
A
CDX2
NANOG
SOX17
DMSO
Reversine
AZ3146
50 µm
B
DMSO
Reversine
AZ3146
Number of cells
P = 0.4609
P = 0.0001
P = 0.0001
P = 0.3256
P = 0.0001
P = 0.001
P = 0.2132
P = 0.0044
P = 0.0560
P = 0.1256
P = 0.0001
P = 0.0001
Total
CDX2
NANOG
SOX17
C
Aggregation chimeras
from 2-cell stage embryos
~72h
culture
D
DMSO/AZ3146 chimeras
Reversine/DMSO
Reversine/AZ3146 chimeras
Half embryo
2 stacks
50 um
CDX2
SOX17
NANOG
E
D/AZ (n=9)
R/AZ (n=21)
D/R (n=10)
% of aneuploid cells
Total
CDX2
NANOG
SOX17

Figure S. 6

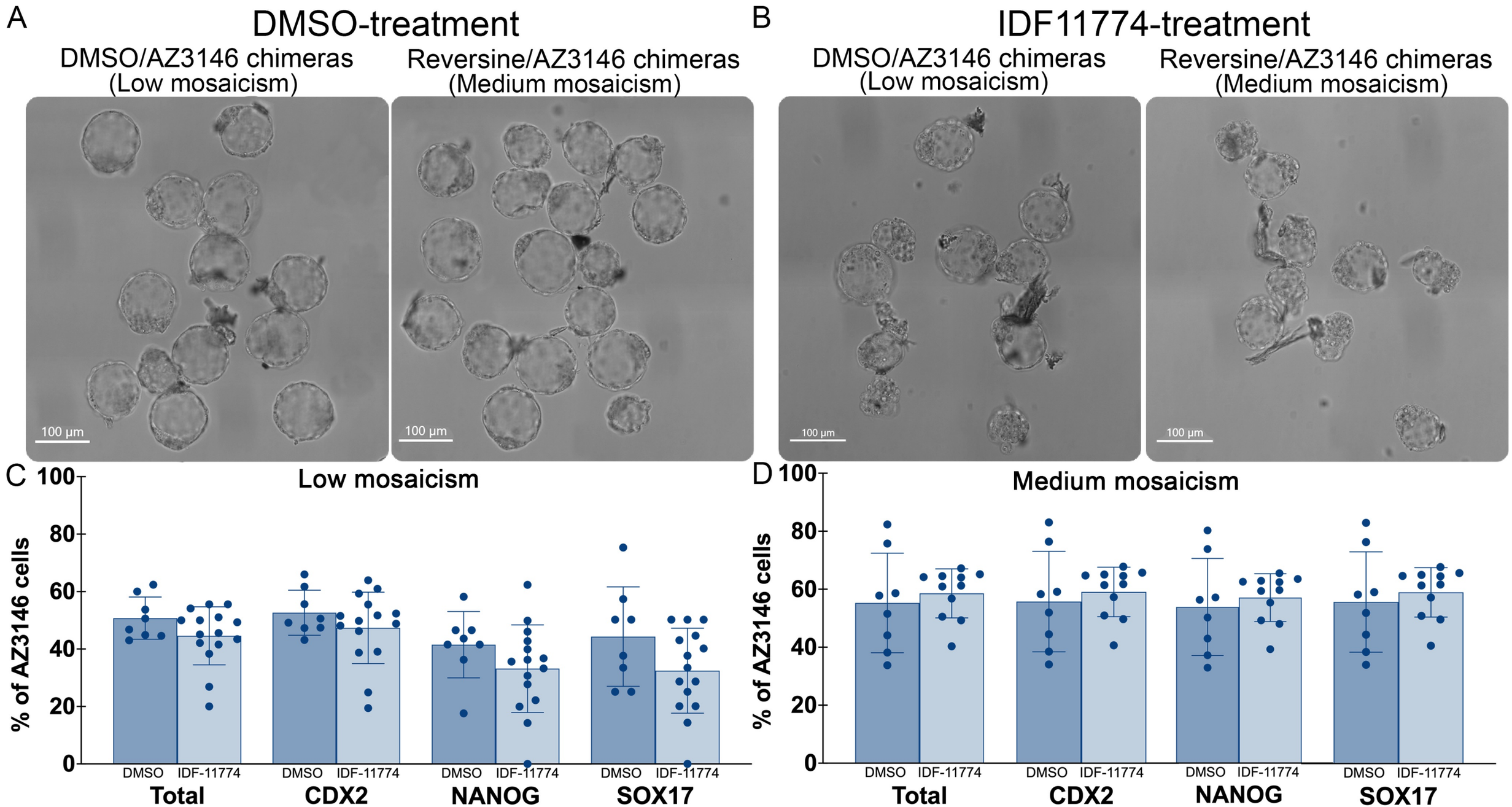
A
DMSO-treatment
DMSO/AZ3146 chimeras
(Low mosaicism)
Reversine/AZ3146 chimeras
(Medium mosaicism)
100 µm
100 µm
B
IDF11774-treatment
DMSO/AZ3146 chimeras
(Low mosaicism)
Reversine/AZ3146 chimeras
(Medium mosaicism)
100 µm
100 µm
C
Low mosaicism
% of AZ3146 cells
100
80
60
40
20
0
DMSO
IDF-11774
Total
CDX2
NANOG
SOX17
D
Medium mosaicism
% of AZ3146 cells
100
80
60
40
20
0
DMSO
IDF-11774
Total
CDX2
NANOG
SOX17